Quantifying Uncertainty in Sustainable Biomass and Production of Biotic Carbon in Enceladus' Notional Methanogenic Biosphere

Peter M. Higgins, Weibin Chen, Christopher R. Glein, Charles S. Cockell, Barbara Sherwood Lollar

JGR Planets

RESEARCH ARTICLE
10.1029/2023JE008166

Quantifying Uncertainty in Sustainable Biomass and Production of Biotic Carbon in Enceladus' Notional Methanogenic Biosphere

Peter M. Higgins[1], Weibin Chen[1], Christopher R. Glein[2], Charles S. Cockell[3], and Barbara Sherwood Lollar[1,4]

[1]Department of Earth Sciences, University of Toronto, Toronto, ON, Canada, [2]Space Science Division, Southwest Research Institute, San Antonio, TX, USA, [3]UK Centre for Astrobiology, School of Physics and Astronomy, University of Edinburgh, Edinburgh, UK, [4]Institut de Physique du Globe de Paris (IPGP), Université Paris Cité, Paris, France

Key Points:

- Spatial habitability on Enceladus is not guaranteed, and additional modeling parameters are needed to evaluate possible vacant habitats
- Cell turnover is important for life detection missions and can be constrained more tightly than total biomass
- Abiotic to biotic ratios of space plume carbon are critical as biosignatures and for assessing the scale of Enceladus' notional biosphere

Supporting Information:

Supporting Information may be found in the online version of this article.

Correspondence to:

P. M. Higgins,
pete.higgins@utoronto.ca

Citation:

Higgins, P. M., Chen, W., Glein, C. R., Cockell, C. S., & Sherwood Lollar, B. (2024). Quantifying uncertainty in sustainable biomass and production of biotic carbon in Enceladus' notional methanogenic biosphere. *Journal of Geophysical Research: Planets*, *129*, e2023JE008166. https://doi.org/10.1029/2023JE008166

Received 17 OCT 2023
Accepted 5 MAR 2024

Abstract Beneath Enceladus' ice crust lies an ocean which might host habitable conditions. Here, the scale and productivity of a notional Enceladean methanogenic biosphere are computed as a function of the core-to-ocean flux of hydrogen and the ratio between abiotic and biotic methane in Enceladus' space plume. Habitats with an ocean-top pH range of 8–9 have up to 40%–60% probability of being energy-limited. Those at pH > 9 are increasingly uninhabitable, and those <8.5 are increasingly likely to host exponential growth, possibly leading to compositional inconsistencies between the ocean and Cassini gas observations. In those cases, energy-based habitability models cannot infer an inhabited Enceladus consistent with both Earth life and Cassini measurements without including additional microbial growth limiters such as nutrient limitation, toxicity, or spatial constraints. If methanogens are isolated to a 350 K seafloor habitat and consume 10 mol s^{-1} of H_2, the most probable biomass is 10^3, $10^{3.7}$ kg C with ocean-top pH 8,9, respectively. Biomass production consistent with space plume fluxes is 10^4–10^6 kgC yr^{-1}—milligrams of cellular carbon per kilogram of H_2O ejected—but requires that >50% of the space plume methane is biotic. Alternative scenarios are presented, and biomass is generally lower when habitat temperature is higher. Ocean biomass density cannot yet be reliably estimated owing to uncertainties in the scale and physicochemical properties of Enceladus' putative habitats. Evaluating abiotic to biotic ratios in plume methane and organic material could help identify false negative results from life detection missions and constrain the scale of an underlying biosphere.

Plain Language Summary The Cassini spacecraft observed energy and nutrient sources for life erupting from a water ocean below the icy exterior of Saturn's moon Enceladus. Future spacecraft planned for Enceladus, Europa and Titan will obtain similar measurements in greater detail. In this work, we calculate the probability that different suites of environments inside Enceladus' ocean are habitable for methanogens, an ancient type of organism which may be able to survive there. Three scenarios are possible: uninhabitable, habitable, and energy-saturated. Next, we extend this calculation to show that the possible biosphere is small but productive. Microbial waste, generated at the seafloor, could be ejected from the ocean and consequently snow down onto Enceladus' surface. Mass spectrometers on future spacecraft could constrain these possibilities further and may be critical to inferring biosignatures when cell densities are too low to detect.

1. Introduction

Below Enceladus' ice crust lies a water ocean which is alkaline, saline, and may be habitable (Higgins et al., 2021; Iess et al., 2014; Thomas et al., 2016; Waite et al., 2009, 2017). An "ocean plume" is thought to emerge from the southern seafloor (Choblet et al., 2017; Steel et al., 2017) traveling to the top of the ocean where a "space plume" of ice and gas erupts from the south polar region, extending for thousands of kilometers (Porco et al., 2006; Villanueva et al., 2023). The Cassini spacecraft analyzed samples of this space plume, which contained myriad salts, silica, organics, and gases (Bouquet et al., 2017; Hsu et al., 2015; Khawaja et al., 2019; Peter et al., 2023; Postberg et al., 2009, 2018, 2023; Waite et al., 2009, 2017). Among the gases were H_2, CO_2, and CH_4, the chemical species involved in the ancient hydrogenotrophic methanogenesis metabolism (Waite et al., 2017). This discovery spurred a flurry of astrobiological analyses to investigate whether the ocean is habitable, if so how much biomass it could sustain, and how future instrument design can best constrain a positive or negative life detection result (e.g., Affholder et al., 2021, 2022; Cable et al., 2020, 2021; Glein & Waite, 2020; Glein et al., 2015; Higgins et al., 2021; Porco et al., 2017; Ray et al., 2021; Roche et al., 2023; Smith et al., 2020; Steel

et al., 2017; Waite et al., 2017). Such analyses are critical for solar system astrobiology as recently described in the National Academies of Science Engineering and Medicine Decadal Survey for Planetary Sciences and Astrobiology (NASEM, 2022) and Enceladus in particular is one of the most important and exciting targets because of its putative habitability (Hendrix et al., 2018).

Although Enceladus' subsurface ocean is well characterized compared to other extraterrestrial ocean worlds, its possible parameter space is broad and uncertainties in key parameters such as pH or concentration of dissolved H_2 span both energetically habitable and uninhabitable conditions (Higgins et al., 2021). This habitability criterion is met when the Gibbs free energy ΔG [J mol^{-1}] extracted by a microbial metabolism can be accessed at a sufficient rate (power supply, $\hat{P}_s$ [W cell^{-1}]) to overcome the power demand associated with survival $\hat{P}_M$ [W cell^{-1}] (Hoehler, 2007). Higgins et al. (2021) took a useful first step by elucidating the geochemical controls on the energetic habitability of Enceladus seawater across the breadth of its observationally constrained parameter space, but did not quantitatively evaluate the probability of energy-limited or energy-saturated habitability and associated sustainable biomass.

Here, habitability is extended to a three-tier classification:

(A) *Uninhabitable*. There is not enough energy available to meet the demands of cell homeostasis: $\hat{P}_S < \hat{P}_M$
(B) *Energetically habitable and energy controls growth rate*. There is enough energy available to survive, but the rate at which the organism can access this energy will limit its growth.
(C) *Energetically habitable and energy may not control growth rate*. Life appears able to grow and the available energy gradients exceed those needed for exponential growth. The system cannot be both in steady state and consistent with the ocean composition as derived from the Cassini measurements unless there are alternative growth limiting factors such as nutrient limitation, substrate sequestration, toxicity, spatial limitations, or metabolic inefficiencies. In other words, in this condition, habitability models *cannot infer* an inhabited Enceladus consistent with *both* Earth life *and* Cassini observations *without* including additional microbial growth limiters.

This provides only an instantaneous habitability assessment informed by the in situ chemical disequilibrium (Cockell et al., 2021; Higgins et al., 2021), but biospheres can only be sustainable for long periods when there is a continuous supply of energy and nutrients (Cockell et al., 2024). Such production is expected to be ongoing on Enceladus, although the exact internal production rates and mechanisms remain unclear (e.g., Daval et al., 2022; Vance et al., 2016; Zandanel et al., 2021). In consequence, modeling efforts of the total biosphere within a notionally inhabited Enceladus produce wide-ranging estimates spanning several orders of magnitude (e.g., Affholder et al., 2022; Porco et al., 2017; Ray et al., 2021; Steel et al., 2017). In this work, the probability that each habitability classification above is met under different Enceladean temperature and pH conditions is determined using the broad ocean parameter space from Higgins et al. (2021). The model is also extended to approximate microbial energy fluxes in hydrothermal environments on Enceladus. Distributions of steady state biomass and cell turnover are then estimated per mole of microbial H_2 consumption, so that they can be scaled, as rates of energy and nutrient provision on Enceladus are constrained.

The total standing biomass and cell turnover can be estimated based on the methane flux observed by a spacecraft. However, such an estimation requires differentiating biotic (e.g., directly produced by biology) from abiotic (formed non-biologically) methane. Carbon/hydrogen stable isotopic signatures (e.g., Sherwood Lollar et al., 2008; Warr et al., 2021) have suggested that various water-rock interactions (e.g., Fischer-Tropsch Type reactions; (Etiope & Sherwood Lollar, 2013)) may produce methane on Earth. These interactions and primordial and thermogenic (organic-derived) sources of methane may also be plausible on Enceladus, though their extent remains unknown. Here, a ratio of abiotic to biotic carbon in the form of methane $R_{ab:b}$ is introduced to provide a constraint on the overall scale and productivity of Enceladus's notional methanogenic biosphere. When $R_{ab:b}$ is 0 it provides the maximally inhabited ocean endmember (i.e., all methane is biotic), and when it is infinite it represents the uninhabited endmember. This provides a framework for interfacing future observations and modeling work to constrain the broad habitability and notional biomass space expected for Enceladus. The model is inferred from space plume observations and ocean models and can be extended to Europa and Titan to interpret measurements from Europa Clipper, Juice, Dragonfly, and the James Webb Space Telescope.

Table 1
Parameter Spaces Used for the Monte Carlo Habitability, Biomass and Turnover Model

Parameters outside MC model	Symbol	Range used	Reference(s)
Temperature	T	273–393 K	Various[a]
Pressure	P	1 bar	Various[b]
Bulk ocean pH	pH_{bo}	7–10	Various[c]
Methanogen power demand	$\hat{P}_M^{2\%}$, $\hat{P}_M^{TOM}$	$\hat{P}_M^{2\%}(T)$, $\hat{P}_M^{TOM}(T)$ W cell^{-1}	Lever et al. (2015) and Higgins and Cockell (2020)
Parameters inside the MC model	**Symbol**	**Range used**	**Reference(s)**
Space plume volume mixing ratio of CH_4:H_2O	$\Lambda_{CH4:H2O}$	0.2% ± 0.1	Waite et al. (2017)
Space plume volume mixing ratio of H_2:H_2O	$\Lambda_{H2:H2O}$	0.9% ± 0.5	Waite et al. (2017)
Space plume volume mixing ratio of CO_2:H_2O	$\Lambda_{CO2:H2O}$	0.55% ± 0.25	Waite et al. (2017)
Concentration of Cl^-[d]	$[Cl^-]$	0.05–0.2 mol kg^{-1}	Postberg et al. (2009)
log10 methanogenesis rate constant k_M[e]	$\log_{10} k_M$	[(−7)–0] ± 1[b]	Higgins and Cockell (2020)

Note. Distributions were all drawn as uniform between the ±values. Ranges and distributions as compiled and discussed by Higgins et al. (2021), or the habitable ranges therein. [a]While hydrothermal temperatures on Enceladus could be much higher than this, temperatures greater than 120°C (or 393 K) are not considered here as they are close to the currently accepted upper limit of Earth life (Takai et al., 2008). [b]Modeling pressure remained at 1 bar (or the saturation pressure for water then temperature was larger than 373 K) for simplicity, on the assumption dissolved gases do not exsolve where life would be. The effect of pressure on dissolved gas bioavailability was investigated separately and this assumption may not be valid at low pressures (Section 3.2). Some of the methanogen growth data were from species cultivated up to 100 bar (Higgins, 2022). [c]pH_{bo} range restricted to 7–10, capturing the scope of putative habitable conditions from Higgins et al. (2021), with 7 as a highly habitable endmember and 10 as a likely uninhabitable endmember. Calculations were performed at intervals of 0.2 between 8 and 9 and 0.5 between 7 and 10. [d]The concentration of Cl^- was used to estimate the molality of DIC. The uniform distribution of Cl^- was drawn in log10 space. To evaluate dissolved gas bioavailability on a more saline Enceladus, case studies up to 0.4 mol kg^{-1} were conducted (Section 3.2). [e]Rate constants calculated by Higgins and Cockell (2020) were based on hydrogenotrophic methanogens in the exponential phase under optimal conditions and varied with temperature. Uncertainty in this value at any temperature is accurately captured by ±1 unit in log10-space.

2. Methods Overview

The habitability and biomass potential of a system can be estimated using its energy and nutrient availability (e.g., Higgins & Cockell, 2020; Hoehler, 2007). Hydrogenotrophic methanogens obtain their energy, in the simplest case, by consuming the dissolved gases CO_2 and H_2, producing CH_4 in the overall reaction:

$$CO_2 + 4H_2 \leftrightharpoons 2H_2O + CH_4 \quad (1)$$

Higgins et al. (2021) used the Enceladus ocean's inferred composition to assess its instantaneous habitability, but to constrain the total standing biomass and possible growth/removal rates of resident organisms, the supply of energy and nutrients is needed.

2.1. Geochemical Model

The heated seawater (HSW) geochemical model from Higgins et al. (2021) based on the Na-Cl-CO_2-O-H carbonate speciation from Glein and Waite (2020) and dissolved gas model from Waite et al. (2017) was recreated, with minor computational updates to maximize the output and analysis of chemical parameters. A Pitzer model (Harvie et al., 1984) was used with the PHREEQC.dat database, improving accuracy in the activity coefficients of dissolved species. In this geochemical model, the composition of major salts NaCl, $NaHCO_3$, and Na_2CO_3 were estimated for an input value of $[Cl^-]$, which is then matched to a probable associated DIC from ice grain measurements (Postberg et al., 2009; Waite et al., 2017). A carbonate speciation was performed at 273.15 K, estimating the concentration of dissolved carbonate species, including CO_2(aq). To estimate the composition at elevated temperature, the speciation procedure was repeated at the desired temperature from this 273.15 K starting point. To compute the activities of dissolved gases H_2 and CH_4, it was assumed that the number ratios between these species relative to CO_2 are similar in the bulk ocean relative to the space plume (Waite et al., 2017). This relationship remains unclear, and it is possible that the gases are depleted in transit (Fifer et al., 2022). The mixing ratios Λ between gases and water based on measurements from Cassini's Ion Neutral Mass Spectrometer were compiled by Waite et al. (2017) and are summarized in Table 1.

The saturation indices (SI) of CO_2 and H_2 were estimated. This quantity is $\log Q_p/K_p$, where Q_p and K_p are the reaction quotient and equilibrium constant, respectively, of the exsolution reactions. It determines their tendency to exsolve in given conditions. The effects of pressure on the speciation up to 100 bar (approximately the maximal seafloor pressure at the ocean's deepest point under minimal ice thickness (Higgins et al., 2021)) were also considered, but as these were found to be insignificant to the activities of the metabolites, all biological analyses reported below were performed at 1 bar (approximately a minimal ocean-top pressure under a few kilometers of ice) unless otherwise indicated. Pressure variability does affect the solubility of dissolved gases and hence their SI and bioavailability, as discussed in Section 3.2. Alternative models were tested, including a Helgeson-Kirkham-Flowers-type speciation model (Helgeson et al., 1981; Tanger & Helgeson, 1988) using the slop07.dat SUPCRT92 database (Johnson et al., 1992) and scenarios where the gases were or were not allowed to equilibrate with the aqueous solution. All speciation calculations were performed using the reaktoro package for chemical systems (Leal, 2015). Text S1 in Supporting Information S1 summarizes the full speciation methodology and discusses these tests.

The most conservative habitability estimate, the HSW model, was used unless stated otherwise. One limitation of the HSW approach is that it does not consider significant chemical differences between seawater in the bulk ocean and hydrothermal fluid (HF). The difference in activities of H_2, CO_2, and CH_4 influences the viability of hydrogenotrophic methanogenesis. The ratio between HF and SW in Enceladus' ocean plume could be between 1:3 (Affholder et al., 2022) and 1:10 (Steel et al., 2017). If the H_2 and CH_4 in the ocean plume come exclusively from this HF, the concentrations of these gases in this HF could be up to 4 or 11 times larger than their values in the ocean plume. To conservatively explore the habitability of HF on Enceladus, case studies were added with the H_2 and CH_4 gas concentrations increased by 10 times. These HF endmembers were then compared to the HSW results to obtain a first approximation of how their habitability differs from the HSW cases. Several additional geochemical differences between these fluids may also affect their habitability (Glein et al., 2018), but this analysis will provide information about how energetic availability for life might be different between HF and SW on Enceladus.

2.2. Habitability, Biomass and Cell Turnover Model

Habitability is an organism-specific binary property (i.e., an environment is either habitable or uninhabitable to a given organism) (Cockell et al., 2019), and in this work habitability refers to whether a given set of conditions allows hydrogenotrophic methanogens to access enough energy per second $\hat{P}_s$ to overcome the energy expenditure per second necessary to survive (maintenance power, $\hat{P}_M$). This is an instantaneous estimate which needs continual revision as the system evolves. Habitability is assessed here using the bioenergetic model NutMEG (Higgins & Cockell, 2020) which compares the instantaneous $\hat{P}_s$ available to an organism, to the $\hat{P}_M$ associated with its physicochemical environment. A maintenance power associated with temperature-dependent biomass replacement after 2% protein racemization, $\hat{P}_M^{2\%}$ (Lever et al., 2015) was used for the main results in this work. This is a conservative minimal estimate which is generalizable to many microbial species independent of their mean protein length. An exponential growth phase maintenance power $\hat{P}_M^{TOM}$ (Higgins & Cockell, 2020) was also examined for comparison and to represent a maximum value. The true $\hat{P}_M$ experienced by notional methanogens on Enceladus likely lies between these endmembers (Higgins, 2022).

Habitability condition A (Section 1) arises when $\hat{P}_s < \hat{P}_M$. Habitability condition B occurs when $\hat{P}_s > \hat{P}_M$ and the growth rate permitted by that energetic availability (i.e., without alternative limitation) μ [s^{-1}] is less than or equal to the growth rates recorded in empirical studies from terrestrial systems at similar temperatures μ_e [s^{-1}]. Similarly, habitability condition C is met when the permitted growth rate μ [s^{-1}] is greater than μ_e [s^{-1}]. A linear regression of optimal hydrogenotrophic methanogen growth rates with temperature from the phymet2 data set was used to determine μ_e at different temperatures (Higgins, 2022; Higgins & Cockell, 2020; Michał et al., 2018). The growth rate permitted by energetic availability μ was calculated using the numerical biokinetic model described by Higgins and Cockell (2020). In that model, under minimal nutrient limitation, when $\hat{P}_s > \hat{P}_M$ the quantity $\hat{P}_s - \hat{P}_M$ is the power available for growth $\hat{P}_G$ [W $cell^{-1}$]. Over some time interval dt, the rate of change in biomass μ is $\frac{\hat{P}_G dt}{E_{syn}}$ where E_{syn} is the energy required to synthesize biomass. The growth rate μ therefore depends on E_{syn}, $\hat{P}_M$, $\hat{P}_s$, and each of these variables depend on geochemical and geophysical parameters including

temperature, composition, and organismic parameters as discussed in Higgins and Cockell (2020) and Higgins et al. (2021).

In conditions B and C, the steady state biomass B_{ss} [cells] was determined as a function of microbial H_2 consumption J^{bio}_{H2} [mol s^{-1}]:

$$B_{ss} = \frac{J^{bio}_{H2}}{4r_m} \tag{2}$$

where r_m [mol CO_2 s^{-1} $cell^{-1}$] is the cell-specific metabolic rate of microbial methanogenesis, following the stoichiometry of Equation 1. r_m was computed using the molar free energy of methanogenesis ΔG, an Arrhenius-like rate constant of microbial methanogenesis k_M, and the activities of H_2 and CO_2 as described in Higgins and Cockell (2020), with the most appropriate adenosine triphosphate (ATP) yield per mole of CO_2 consumed n_{ATP} (Higgins, 2022). This parameter determines the thermodynamic drive of the microbially mediated reaction (Jin & Bethke, 2007) and the exact value often changes between individual organisms (for methanogens, n_{ATP} is typically between 0.25 and 2.0 (Buan, 2018)). In this work, only the most efficient values of n_{ATP} for a given set of environmental conditions was used. In other words, this assumes that any methanogens are perfectly adapted to their habitat as modeled to extract the most energy possible.

Cell turnover refers to any mechanism of biomass loss such as death, removal from the habitat, or predation. In the steady state, the biomass turnover τ_{ss} [cells s^{-1}] is equal to the rate of biomass production μ such that B_{ss} stays constant:

$$\tau_{ss} = \Gamma B_{ss} = \mu B_{ss} \tag{3}$$

where Γ [s^{-1}] is the death (removal) rate of B_{ss} and μ was estimated using the NutMEG energy-limited microbial growth algorithm as described above (Higgins & Cockell, 2020). The growth rate μ is inversely proportional to the energetic cost of biomass synthesis E_{syn} [J $cell^{-1}$] at first order because E_{syn} determines how many cells can be generated using a given power available for growth (Higgins & Cockell, 2020). As described above, it also depends on $\hat{P}_M$ and $\hat{P}_s$. These dependencies hence carry to Γ by Equation 3. Nutrient limitation was not included and is discussed in Section 4.

In light of uncertainty in H_2 generation on Enceladus and how much of it may be microbially accessible (e.g., Cable et al., 2020; Daval et al., 2022; Steel et al., 2017; Vance et al., 2016), steady state biomass and cell turnover in this work are presented and discussed in terms of sustainable cells per mole of H_2 consumed per second (Equation 4), and cells removed per second per mole of H_2 consumed per second (Equation 5):

$$B^{H2}_{ss} = \frac{B_{ss}}{J^{bio}_{H2}} = \frac{1}{4r_m} \tag{4}$$

$$\tau^{H2}_{ss} = \Gamma B^{H2}_{ss} \tag{5}$$

2.3. Monte Carlo Implementation

The Higgins et al. (2021) parameter space was used as summarized in Table 1 to perform a Monte Carlo [MC] simulation at individual values of temperature T [K], pH in the bulk ocean (pH_{bo} at 273 K), and the temperature-associated maintenance power $\hat{P}_M$ (T). These parameters are examined using independent MC simulations because they are the most important indicators of habitability in Enceladus' ocean (Higgins et al., 2021), and this allows for pH- and temperature-specific probabilities of conditions A, B, and C (P_A, P_B, and P_C respectively). These then extend to probability density distributions of B^{H2}_{ss} and τ^{H2}_{ss}. The MC calculation draws from uniform distributions of space plume gas volume mixing ratios, the microbial methanogenesis rate constant, and ocean chloride concentration [Cl^-] in $\log_{10}$-space, which is coupled to the dissolved inorganic carbon concentration [DIC] (Text S1 in Supporting Information S1) with sample sizes of 25,000. The microbial ATP yield was computed on a case-by-case basis, choosing the most efficient value for the MC ΔG and metabolic rate constant (Higgins, 2022).

2.4. Constraining Biotic Methane Delivery to the Space Plume

If J_{H2}^{bio} is known over a given volume scale of homogeneous T and pH, B_{ss} and τ_{ss} can be computed for that volume (Equations 4 and 5). For a H_2 (CH_4) inflow J_{H2}^{in} (J_{CH4}^{in}) and outflow J_{H2}^{out} (J_{CH4}^{out}) and assuming there are no other notable sinks of these gases in the volume of interest it can be approximated that:

$$J_{H2}^{out} = J_{H2}^{in} - J_{H2}^{bio} \tag{6}$$

$$J_{CH4}^{out} = J_{CH4}^{in} + J_{CH4}^{bio} \tag{7}$$

Methane is involved in and produced by biotic and abiotic processes (e.g., Etiope & Sherwood Lollar, 2013) and the ratio between these flowing out of the volume $R_{ab:b} = J_{CH4}^{abio} / J_{CH4}^{bio}$ could be used to interpret future isotopic analyses of icy moon plume material. Thermogenesis of organic material is not considered in this model, so "biotic" CH_4 here refers only to that generated by microbial methanogens and not subsequently processed aside from plume transit. This ratio can be related to J_{H2}^{bio}. Substituting $R_{out} = J_{H2}^{out} / J_{CH4}^{out}$ into the equations above gives:

$$J_{H2}^{bio} = J_{H2}^{in} - R_{out}\left(J_{CH4}^{in} + J_{CH4}^{bio}\right)$$

Substituting $R_{ab:b}$:

$$J_{H2}^{bio} = J_{H2}^{in} - R_{out} J_{CH4}^{bio}(R_{ab:b} + 1)$$

Finally, as four moles of H_2 are consumed for each mole of CH_4 produced in hydrogenotrophic methanogenesis (Equation 1), $J_{CH4}^{bio} = 0.25 J_{H2}^{bio}$:

$$J_{H2}^{bio} = J_{H2}^{in} - 0.25 R_{out} J_{H2}^{bio}(R_{ab:b} + 1)$$

which rearranges to

$$J_{H2}^{bio} = \frac{J_{H2}^{in}}{1 + 0.25(1 + R_{ab:b}) R_{out}} \tag{8}$$

This study assumes that methanogen habitats on Enceladus are the only major sink of H_2 after the mixing of HF and SW. When a range of values for J_{H2}^{in} and $R_{ab:b}$ are provided, their B_{ss} and τ_{ss} can be computed at a given T and pH_{bo}. For R_{out}, the volume mixing ratios in the space plume Λ reported by Waite et al. (2017) were used (Table 1). The total molar output of H_2 was computed by comparing the volume mixing ratio of H_2 and H_2O to the total mass of water ejected from Enceladus (variable at approximately 100–1,000 kg s^{-1} (Cable et al., 2020; Hansen et al., 2011; Teolis et al., 2017; Villanueva et al., 2023)) and is approximately 22–777 mol s^{-1} through Gaussian error propagation of plume gas mixing ratios. $R_{ab:b}$ can take any value between 0 (all CH_4 biotic) and ∞ (uninhabited or no detectable biotic CH_4).

3. Results

3.1. Energy-Limited Habitability Most Probable With a Bulk Ocean pH Between 8 and 9

Figure 1 shows the probability of habitability conditions A, B, and C (P_A, P_B, P_C respectively) at seawater temperatures between 273 and 393 K and pH_{bo} 8–9 and 7–10. The 8–9 pH range both captures the broad consensus on the bulk ocean pH of Enceladus' ocean as constraints have tightened over recent years (Fifer et al., 2022; Glein & Waite, 2020; Hsu et al., 2015; Postberg et al., 2009) and suggests the largest values of P_B throughout these temperatures. $\hat{P}_S$ is more likely to exceed $\hat{P}_M^{2\%}$ at higher temperatures than it is at lower temperatures, mainly owing to the temperature dependence of k_M. The probability peaks in Figure 1b are due to initially low $\hat{P}_S$ which increases with temperature at a steeper gradient than $\hat{P}_M^{2\%}$ in Enceladus-like conditions. As this difference grows, it becomes increasingly probable that the system is not energy limited and microbial growth must either be exponential or quenched in alternative ways such as by nutrients, heavy metals, toxicity, or spatial

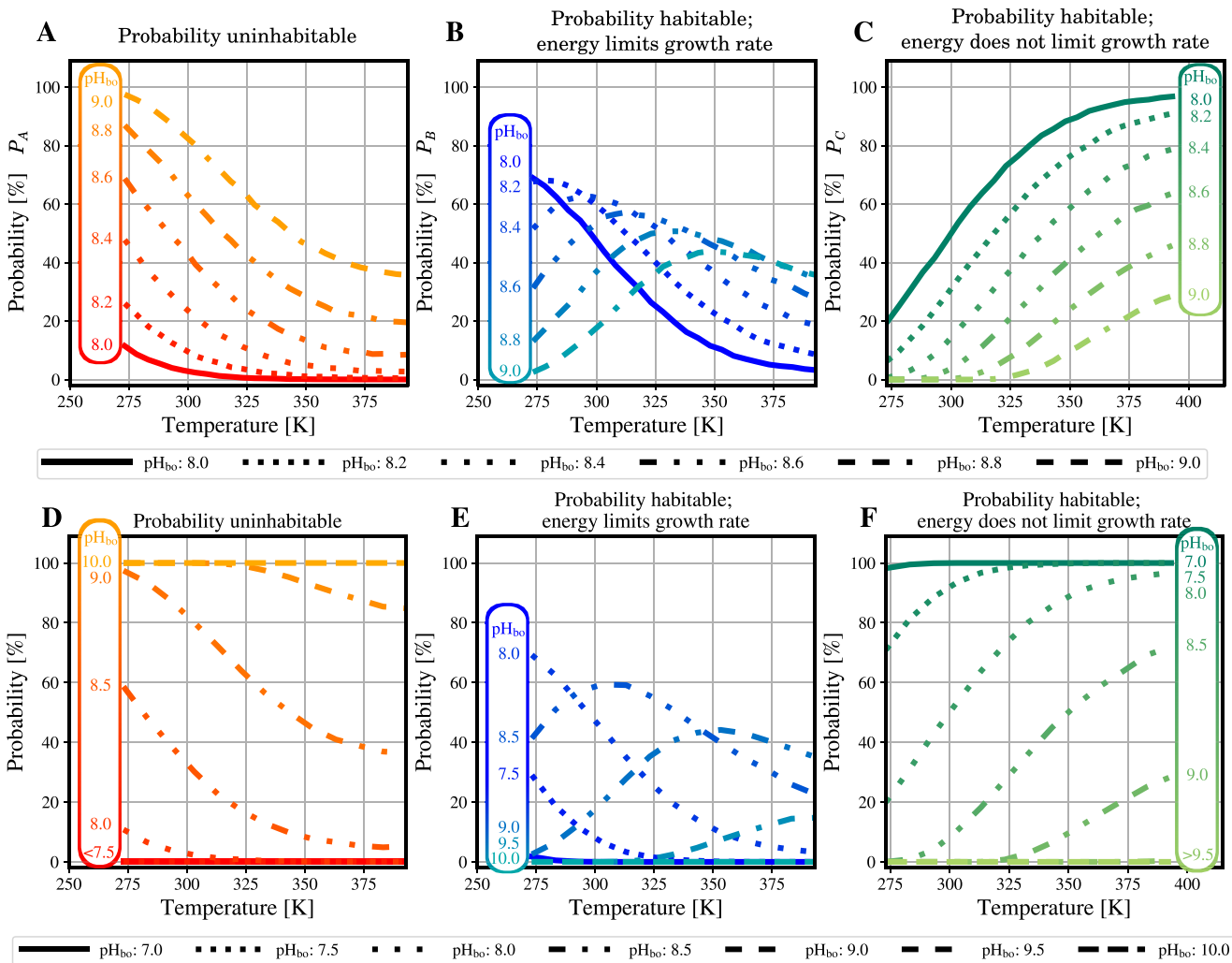

Figure 1. The probabilities of uninhabitability, habitable with energy-controlled growth and habitable where growth is not controlled by energy (conditions A, B, C; panels a, b, c, respectively) for bulk ocean pH values between 8 and 9 at 1 bar, between 273 and 393 K (the currently understood thermal limit for life is ~395 K). At each pH_{bo} and temperature value, the sum of probabilities P_A, P_B, and P_C equals 100%. These probabilities are taken from the MC distributions as the fraction of samples which meet the A, B or C criteria. Panels (d–f) show the same results over a wider pH range of 7–10. Legends correspond to the three panels above them only. All panels use the 2% racemization microbial maintenance, reflecting theoretical estimates of the minimal power demand. Alternative figures using the maximal maintenance power are shown in Figure S1 of the Supporting Information S1, and with increased dissolved gas concentration in Figure S2 of the Supporting Information S1.

bioavailability (e.g., the ability for the organisms to access and make use of CO_2(aq) and H_2(aq) fluxes). These limiters could reduce the growth rate and shift the result from habitability condition C to B or A (Higgins & Cockell, 2020). Alternatively, the null hypothesis under condition B or C is that Enceladus' rock-water interface is simply a vacant habitat (i.e., theoretically habitable, but uninhabited because Enceladus lacked an origin of life or transfer of life to the moon).

Ocean-top pH values >9 are more likely to be uninhabitable than habitable at most temperatures, and when $pH_{bo} > 9.5$, almost the entire parameter space is uninhabitable (Figures 1d–1f). Conversely, habitability condition C becomes more probable throughout the parameter space with increasing temperature when $pH_{bo} < 8$, capturing 100% of MC samples above 300 K at pH 7 despite the conservative [H_2]. Because constraints on Enceladus' nutrient content are not yet well understood, previous studies reasonably assumed that energy availability would be the biomass limiting step in an inhabited Enceladus (e.g., Affholder et al., 2021, 2022; Higgins et al., 2021; Ray et al., 2021). However, the results presented here suggest that if future refinements of ocean chemistry predict a bulk ocean pH of 7–8, non-energetic growth limitation mechanisms would be required for observations to be compatible with the presence of methanogenic life. Alternatively, assuming that estimates of bulk ocean pH

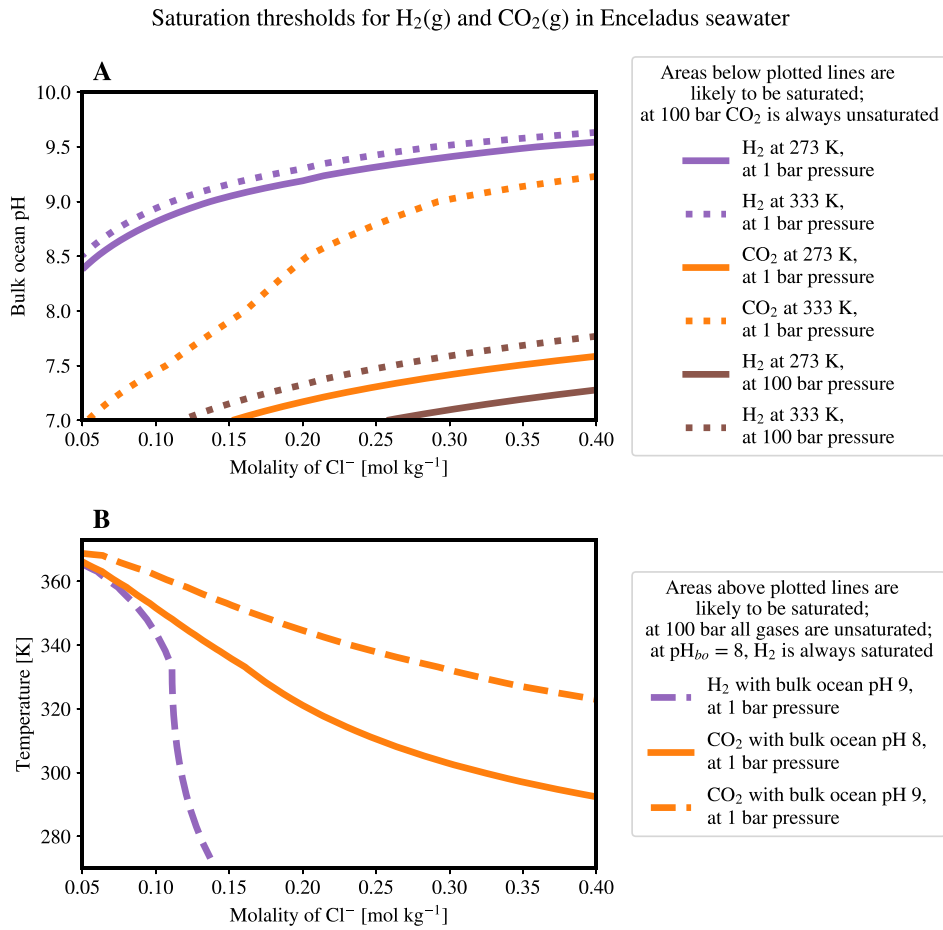

Figure 2. Saturation thresholds for H_2 and CO_2 in Enceladus seawater. These panels show the combinations of bulk ocean pH and [Cl] (a) and temperature and [Cl] (b) that correspond to a saturation index of 0. The lines therefore show the boundaries across which the dissolved gases change between being likely unsaturated and being likely saturated. In panel (a), lines indicate different gases, pressures of either 1 or 100 bar, and temperatures of either 273 or 333 K. Areas below the plotted line are more likely to be saturated in panel (a). In panel (b), lines indicate different gases, pressures of either 1 or 100 bar, and bulk ocean pH values of either 8 or 9. Areas above the plotted line are more likely to be saturated in panel (b). All dissolved gas concentrations in this figure were estimated using their nominal space plume mixing ratio with CO_2 (Table 1; Waite et al. (2017)).

remain between 8 and 9, a sustainable energy-limited methanogen biosphere remains a distinct possibility (peaks in P_B of 40%–60%). This interpretation could be different if the relationship between [H_2] and pH is more complex than modeled here.

The transition between habitability conditions A → B→ C when using the more conservative maximal microbial maintenance $\hat{P}_M^{TOM}$ is narrower than that with $\hat{P}_M^{2\%}$ because the power demand is larger. Using $\hat{P}_M^{TOM}$, $P_A > 50\%$ when $pH_{bo} > 8$ and $P_A = 100\%$ when $pH_{bo} > 9$ (Figure S1 in Supporting Information S1). The microbial trade-offs around $\hat{P}_M$ and $\hat{P}_S$ at Enceladus-like T and pH_{bo} were examined in detail by Higgins et al. (2021).

3.2. Reduced Bioavailability of H_2 and CO_2 Near Ice-Water Interface and in a Highly Saline Ocean

When pH_{bo} is 7–8 and [Cl^-] > 0.1 mol kg^{-1}, the bioavailability of dissolved gases H_2 and CO_2 is lower than that captured by the MC samples because the geochemical model suggests that they should partially exsolve if allowed to equilibrate, possibly due to salting-out effects. The gases' SIs vary with temperature, pressure, dissolved gas concentration and salinity as visualized in Figures S5–S8 of the Supporting Information S1. Figure 2 summarizes some combinations of pressure, temperature, bulk ocean pH and [Cl^-], which correspond to a SI of 0 for CO_2 and H_2. This is the threshold which straddles likely unsaturated and saturated states. The figure shows different case

studies: at temperature 273 and 333 K (Figure 2a) and at bulk ocean pH values of 8 and 9 (Figure 2b). The key thresholds are summarized below:

- H_2 at 1 bar, 273K: Supersaturated when pH_{bo} is <8.5, throughout salinity range.
- H_2 at 100 bar, any T: Becomes saturated when pH_{bo} is 7–8, $[Cl^-] > 0.2$ mol kg^{-1}.
- CO_2 at 1 bar, 273K: Becomes saturated when pH_{bo} is 7–8, $[Cl^-] > 0.1$ mol kg^{-1}.
- CO_2 at 100 bar: Remains dissolved in all cases.

Within the Enceladus parameter space pH is the dominant contributor to the SIs, but elevated salinity also increase the likelihood of exsolution in all cases. As temperature increases, exsolution of CO_2 becomes less favorable faster than exsolution of H_2 (Figure 2a) because the relationship between $\log K_P$ for CO_2 exsolution has a stronger gradient with temperature. At 1 bar and 273K, the maximum bioavailable concentrations of dissolved H_2 and CO_2 are approximately 0.1 and 10 mmol kg^{-1}, respectively. At 100 bar the maximum bioavailable concentration of H_2 is approximately 30 mmol kg^{-1}, and all CO_2 is bioavailable. It follows that at environments near the top of the ocean at pH_{bo} 7–9, ~1 bar, the MC parameter space may overestimate the bioavailable energy. Figure 2a shows that this threshold is met for H_2 around pH 8.5–9.5 as a function of $[Cl^-]$, so may artifically increase the modeled probability of habitability at bulk ocean pH values below this range. On the other hand, at a ~100 bar ocean floor, even if the habitat is saturated with H_2, that alone is unlikely to tip the balance toward an uninhabitable result. In Figure 2a, at 100 bar, the H_2 in a 333 K habitat is unlikely to be saturated unless the bulk ocean seawater pH is less than 7.5. If Enceladus' ocean is more saline than 0.2 mol kg^{-1} $[Cl^-]$, maximum bioavailability due to saturation of H_2 and CO_2 could be further reduced. To test this, these calculations were repeated with salinity up to 0.4 mol kg^{-1} $[Cl^-]$, but this showed very little effect on the ranges described above (Figures S5–S8 in Supporting Information S1).

3.3. Steady State Cell Turnover Is More Tightly Constrained Than Steady State Biomass

Figure 3 shows probability distributions of steady state biomass and cell turnover in the computed habitable space on Enceladus at various temperatures and at pH_{bo} 8 and 9. These were generated using only the habitable space (conditions B and C), so while they integrate to 1, they only represent a certain percentage of the possible parameter space, which is noted next to each distribution. pH_{bo} values >9 were modeled but not shown here due to the high probability of uninhabitability, and those <8 increasingly require additional growth limiting mechanisms. The top four panels use $\hat{P}_M^{2\%}$ at pH_{bo} 8 and 9 and the bottom two panels use $\hat{P}_M^{TOM}$ at pH_{bo} 8. Distributions of biomass per mole of H_2 consumed appear to increase as temperature decreases. This occurs because when temperature decreases, so does r_m (hence increasing B_{ss} by Equation 4). The methanogens respire more slowly at low temperature, so a higher cell count is needed to consume one mol per second of H_2.

In each configuration, the distribution of biomass turnover rate on Enceladus is more tightly constrained than the amount of biomass itself (i.e., there are narrower peaks in the biomass turnover plots compared to those of the steady state biomass). This arises from including a context-specific removal rate rather than a constant value (Equation 3). For each distribution of biomass and turnover generated, the means and 95% confidence intervals are summarized in Tables S3–S27 of the Supporting Information S1. This includes results for all temperatures, pH_{bo}, maintenance powers, and dissolved gas scaling.

Importantly, biomass turnover throughout the pH 8–9 habitable parameter space is constrained to within $10^{12.5}$–10^{14} cells per mole of H_2 consumed (Figure 3 right-hand-side) and is inversely proportional to the energetic cost of biomass synthesis. This model uses a temperature-dependent theoretical minimum synthesis energy from Higgins and Cockell (2020) (approximately 500 J dry g^{-1} at 298 K) and those in natural/laboratory settings could be up to an order of magnitude larger (McCollom & Amend, 2005). Therefore, these turnover rates could conservatively be as low as 10^{11} cells per mole of H_2 consumed.

Cell turnover may be further reduced in configurations which meet habitability condition C. Configurations generating this result become increasingly probable as temperature increases (Figure 1) and may explain artifacts where the steady state biomass is smaller than the rate of biomass turnover. For example, in the top two panels of Figure 3 at 393 K, in some scenarios a steady state biomass of less than 10^{10} cells $(\text{mol s})^{-1}$ is expected but the smallest turnover is $10^{12.6}$ cells $(\text{mol s})^{-1}$. This is one consequence of a large predicted microbial growth rate arising from excess energy availability and lack of alternative growth limitation in the model. The transition

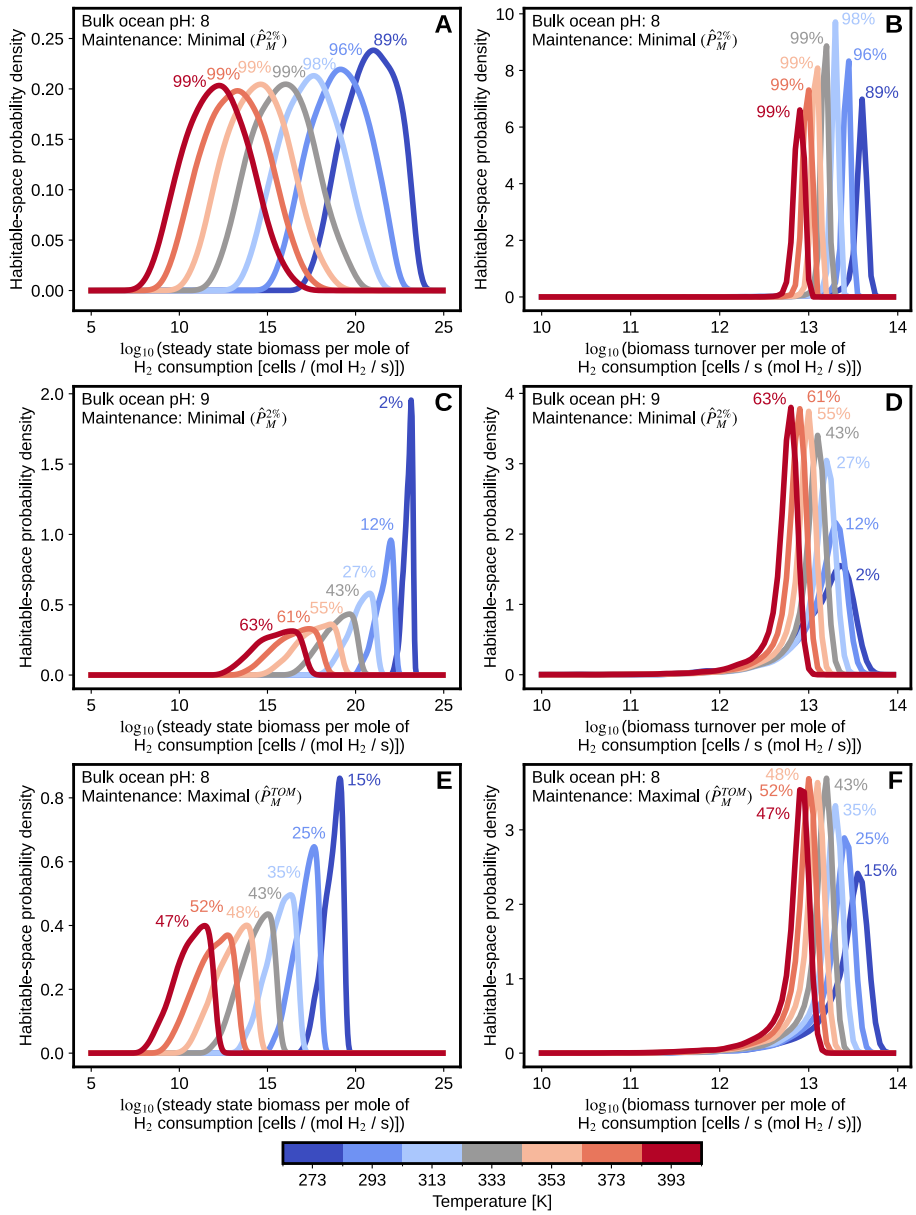

Figure 3. Probability distributions of biomass and turnover in Enceladus' habitable space (e.g., conditions B, C) in Figure 1, with each panel showing distributions at temperatures between 273 and 393 K in intervals of 20 K. Text above the curves indicates the total percentage of the sample that was habitable, and the integral under each individual curve equals 1. This normalization process determines the values on the vertical axes for each panel. Left-hand-side plots (i.e., a, c, e) are of biomass and right-hand-side plots (i.e., b, d, f) are of cell turnover, both per mole of H_2 consumed by methanogens per second. The vertical axes all show probability density and take various ranges between all six plots. Panels (a and b) use a minimal maintenance $\left(\hat{P}_M^{2\%}\right)$ and a bulk ocean pH of 8, panels (c and d) use a minimal maintenance and a bulk ocean pH of 9, and panels (e and f) use a maximal maintenance $\left(\hat{P}_M^{TOM}\right)$ and a bulk ocean pH of 8. The color of the curve indicates the temperature from which each distribution was drawn. Mean and 95% confidence intervals for these distributions are available in Tables S7, S8, and S11 of the Supporting Information S1.

between conditions B and C with temperature is shown in Figure 4 as a reference for when biomass is likely restricted by other mechanisms and turnover may be overestimated.

Figure 4 shows the range of steady state biomass per mole of H_2 consumed per second as predicted by the present model and an alternative method which uses only the available Gibbs free energy ΔG [J (mol H_2)$^{-1}$] and a maintenance power (e.g., Higgins, 2022; Ray et al., 2021):

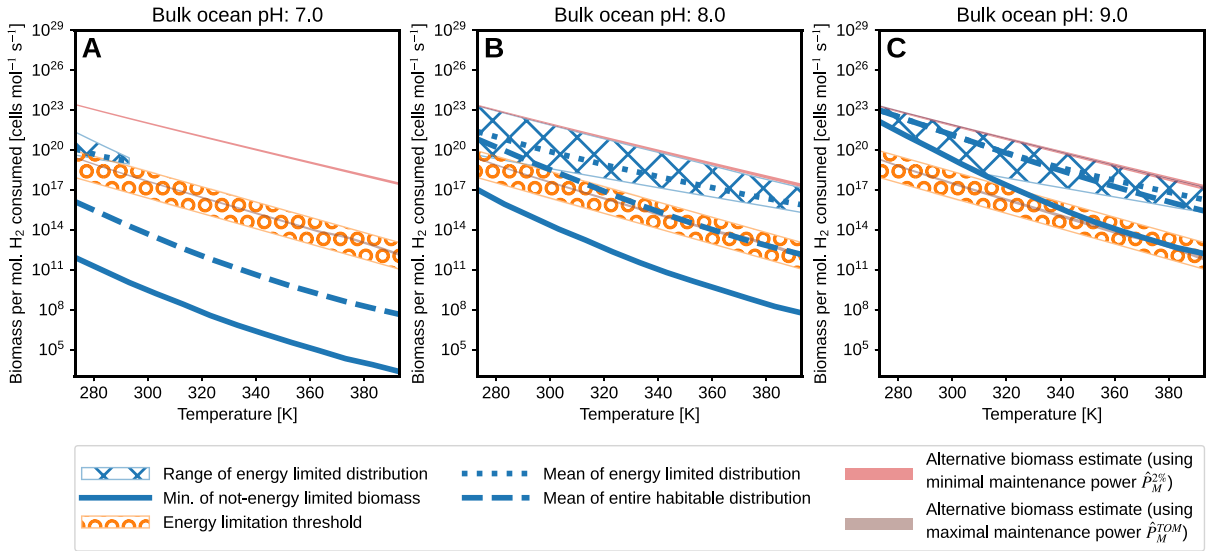

Figure 4. Trends with temperature in the envelope of biomass estimates predicted by the MC model (Figure 3) using a minimal maintenance power at ocean-top pH 7, 8, and 9. At pH 10 the parameter space is uninhabitable so biomass would be 0. The crosshatched area shows the section of the distribution representing energy-limited biomass (condition B), with the dotted line indicating the mean of that distribution. The dashed line is the mean biomass of the entire habitable distribution (conditions B and C) and the solid line the lower 3σ limit of biomass. The thin red and brown bars represent alternative biomass estimates using minimal and maximal maintenance powers, respectively (Equation 9). The circle-hatched area shows the transition area between energy limited and not-energy limited biomass. At pH_{bo} 7, the energy-limited distribution stops at approximately 300 K. This is because at temperatures higher than this limit, all results are in habitability condition C (Table S3 in Supporting Information S1).

$$B_{alt} = \frac{\Delta G}{\hat{P}_M} \tag{9}$$

Steady state biomass estimates in Figure 4 should be compared with the red bar, which is the result expected using the same maintenance power and variation in ΔG as the MC simulations. Biomasses estimated by the MC model are always less than or equal to this alternative approach. Two reasons for this are:

1. The effect of variation in ΔG on steady state biomass is minor compared to parameters that control microbial kinetic factors, such as $[H_2(aq)]$ (Higgins et al., 2021). This also explains why the dependency of biomass on pH for the alternative method is very minor compared to the MC approach and is difficult to see on a logarithmic scale (Figure 4).
2. Models based only on free energies calculate the highest amount of biomass that can be supported (e.g., incoming power supply divided by maintenance power), neglecting the biomass turnover and energy that must go into regrowth when cells die.

Figure S3 in Supporting Information S1 shows alternative trends in temperature using the maximal maintenance power $\left(\hat{P}_M^{TOM}\right)$ and elevated H_2 and CH_4 concentrations. When energy-limited (dotted lines in Figure 4), MC predicted biomasses are larger than those computed using $\hat{P}_M^{TOM}$ in Equation 9. When $\hat{P}_M^{TOM}$ is used in the alternative method, the alternative biomass estimate still reflects a maximum (Figure S3 in Supporting Information S1).

Also noted in Figure 4 is an energy limitation threshold (shown in hatched orange circles). This is the range of temperature dependent biomasses expected in the transition space from habitability conditions B to C: $1/4r_m^{max}$, where r_m^{max} is the range of maximum metabolic rates of methanogens observed in the laboratory per mole of CO_2 (Higgins, 2022; Higgins & Cockell, 2020; Michał et al., 2018). Steady state biomasses lower than this range are in habitability condition C and are likely limited by alternative mechanisms.

3.4. Enceladus' Ocean Floor May Be Habitable at Bulk Ocean pH Values Up to 9–10 Depending on Mixing With Hydrothermal Fluid

Increasing [H_2] and [CH_4] from plume inferred concentrations, approximating increased mixing with HF, increases H_2 bioavailability. If the ratio of seawater to HF in the ocean plume is 1:10, and a bulk ocean with no HF mixing would have negligible [H_2], the hydrothermal interface with the ocean could conservatively provide a ≈10-fold increase in these dissolved gases. The analyses in Sections 3.1 and 3.3 were repeated with an order of magnitude larger [CH_4] and [H_2]. This increase allows organisms to access the energy at a similar rate as they can in seawater heated to the relevant temperature at one pH_{bo} unit lower, and extends to the habitability probabilities and biomass distributions (Figures S2 and S3; Tables S14–S26 in Supporting Information S1). When pH_{bo} is 9 with elevated [H_2] and [CH_4], the habitability classifications and biomass distributions are qualitatively similar to heated seawater of a bulk ocean at pH 8 (Figures 1 and 3 and Figures S2 and S3 in Supporting Information S1). As well as increased [CH_4] and [H_2], mixing with HF could affect the salinity of the notional habitat. As shown in Section 3.2, highly saline fluids affect the solubility of the methanogenesis species and may reduce their bioavailability; therefore, this habitability enhancement over heated seawater should be considered a maximal endmember.

3.5. Abiotic to Biotic Methane Ratios Inform Cellular Carbon Production Rates

The steady state biomass and biomass turnovers per mole of H_2 consumption per second were converted into total ocean constraints consistent with Cassini observations as a function of $R_{ab:b}$ (Figures 5b–5d), referred to as total standing biomass and total biomass turnover, respectively. For any fixed $R_{ab:b}$ there exists a window of possible J^{bio}_{H2}, J^{in}_{H2} and J^{out}_{H2} values which satisfy the steady state criteria (Equation 8), and by Equations 4 and 5, a window of B_{ss} and τ_{ss}. This window is visualized for $R_{ab:b} = 0$, 1 and 100 in Figure S4 of the Supporting Information S1. Figure 5 constrains the maximum and minimum values of J_{H2} (Figure 5a), τ_{ss} (Figure 5b) and B_{ss} (Figures 5c and 5d) for $R_{ab:b}$ values between 10^{-6} and 10^{6}, representing a spectrum from biotically dominated CH_4 to abiotically dominated CH_4.

Figure 5a shows the maximum and minimum biological H_2 consumption rates alongside the range of required H_2 inflow to the ocean to support that biomass and be consistent with space plume fluxes. This figure has decoupled abiotic H_2 and CH_4 production (e.g., not providing explanation for the source of the abiotic methane), but as the H_2 production in Figure 5a does not change significantly in the context of its uncertainty, even if each mole of CH_4 produced abiotically consumes 4 mol of H_2, the total required H_2 production remains close to the range shown in Figure 5a.

Figure 5b shows maximum and minimum total biomass turnover estimates calculated using the H_2 consumption in Figure 5a and the distributions presented in Figure 3. Four endmember values of τ^{H2}_{ss} were propagated to estimate the total turnover:

(i) Maximum and (ii) Minimum values from the MC model with minimal E_{syn}, which represent most of the habitable range regardless of ocean pH or habitat temperature: 10^{14} and $10^{12.5}$ cells per mole of H_2 per second, respectively.
(iii) Turnover characteristic of an Earth-like thermophilic autotrophic methanogen: 0.4 g cells per mole of H_2 metabolized (*Methanobacterium thermoautotrophicum*; Schönheit et al. (1980)). This translates to $10^{11.6}$ cells per mole H_2 per second for the 10^{-12} g per cell simulated here.
(iv) Conservative minimum estimated from MC results in Section 3.3, which considers the possible inflated cost of biomass synthesis in natural environments: 1×10^{11} cells per mole H_2.

Generalizing these turnovers to the flux of total cellular carbon (e.g., biotic organic matter), which arrives at the top of the ocean, yields a conservative maximum of 10^{4}–10^{6} kg C per year from the ocean for a biotic CH_4 dominated (>50%) space plume. If this cellular carbon flux is conserved into the space plume, its maximum concentration is in the order of mg C per kg of H_2O. This estimate was made by diluting the biotic carbon through the total plume mass output dominated by water (up to 1,000 kg/s, (Cable et al., 2020)). This is equivalent to approximately 10^{9}–10^{11} cells/kg H_2O (10^{6}–10^{8} cells/g). As per uncertainty in H_2 production, the energy requirement of biomass synthesis, weakly constrained concentration/dilution factors, predation or decay, each of these estimates represents tentative maximum limits. They can be revised up or down by several unconstrained factors, discussed further in Section 4.

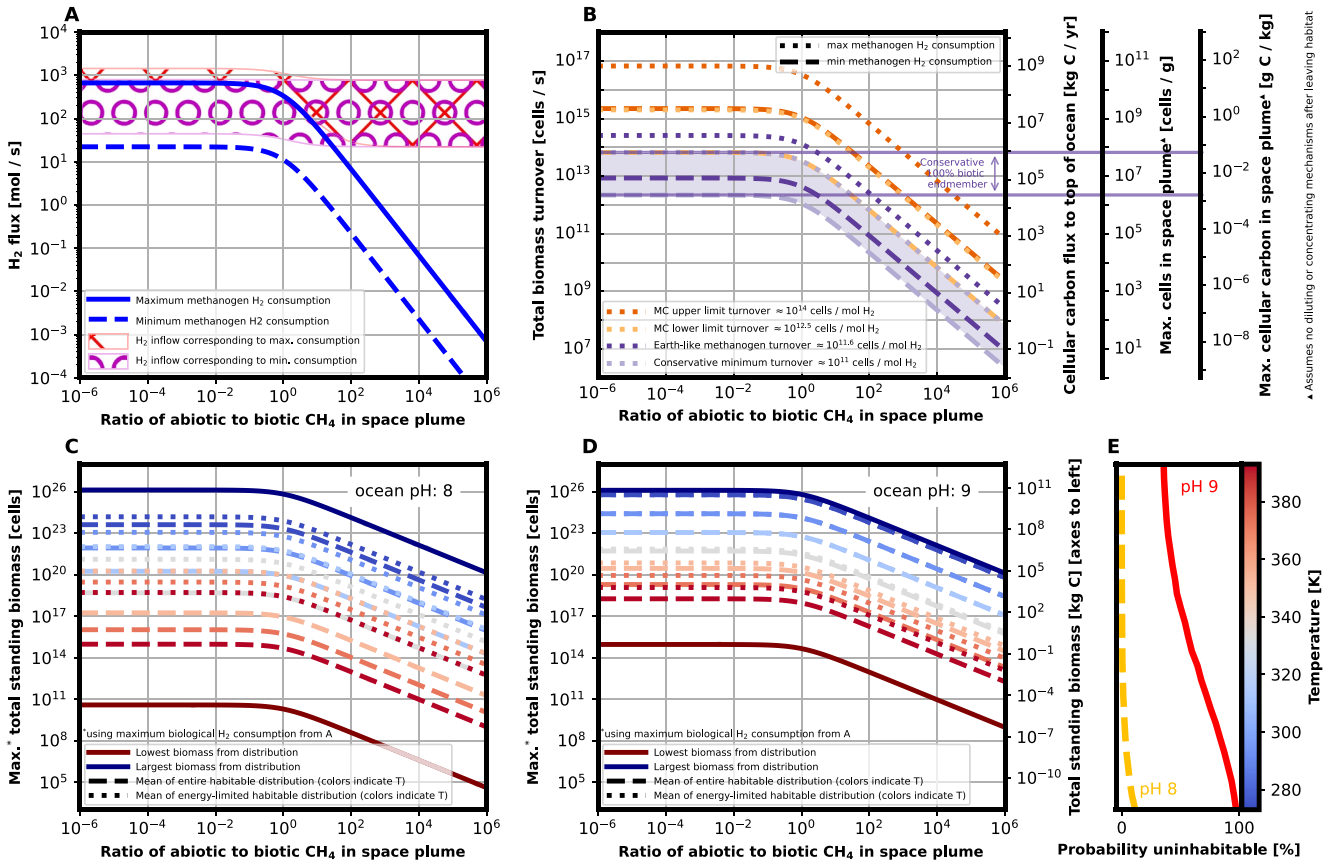

Figure 5. Total standing biomass and biomass turnover in Enceladus' ocean consistent with space plume H_2 and CH_4 fluxes expressed as functions of the ratio of abiotic to biotic methane in the space plume. (a) Ranges of total possible H_2 consumption by methanogens and associated inflow to the ocean required to be consistent with the space plume. (b) Total biomass turnover expected on Enceladus with the H_2 consumption plotted in (a), using four conversions as discussed in the main text. Additional vertical axes convert this turnover into cellular material fluxes to the top of the ocean and into plume material, with the area between the purple lines corresponding to a 100% biotic methane endmember that uses the most reliable and conservative of these turnovers. (c) The mean total standing biomass at various temperatures for a pH 8 ocean under maximal microbial H_2 consumption for the entire habitable distribution (dashed lines) and only the energy-limited habitable distributions (dotted lines). Equivalent biomasses for the minimal H_2 consumption are approximately 35 times smaller. Solid lines show the approximate maximum and minimum total oceanic biomasses informed by Figure 3. (c as d) for ocean pH 9. (e) The probability that a given temperature is uninhabitable at pH 8 or 9 (see Figure 1). The colorbar for (c) and (d) acts as the *y* axis for (e).

Figures 5c and 5d show the total standing biomass on Enceladus required to explain the observation of $R_{ab:b}$ at different temperatures, when pH_{bo} is 8 or 9, respectively, and maximal biological H_2 consumption is assumed (solid line Figure 5a). At first glance, in the biotic CH_4 dominated endmember, maximum standing biomass in the ocean appears to vary between 10^{11}–10^{26} and 10^{14}–10^{26} cells at pH 8 and 9, respectively. However, these ranges were estimated assuming all available H_2 flux is being consumed at the given temperature. The H_2 flux is most likely to be concentrated at or below the seafloor, where temperatures are higher (Cable et al., 2021). A more appropriate maximum endmember in a 350 K habitat, with total H_2 consumption of 1,000 mol s^{-1}, is 10^{20} cells at pH 8 and 10^{21} cells at pH 9, as discussed in Section 4.3. The total modeled energy-limited biomass is larger than the total not-energy-limited biomass because in the energy saturated conditions, each cell is able to consume more H_2 per second due to more favorable biokinetics (i.e., larger r_M in energy-saturated conditions).

The cell density in cells cm^{-3} is not reliably calculable. If the notional biomass is evenly distributed throughout a 273 K ocean with volume of order 10^{16} m^3 (Higgins, 2022; Steel et al., 2017), the corresponding maximum biomass density appears to be 10^{-2} or 10^{-1} cells cm^{-3} for a pH 8 or 9 ocean, respectively. However, this is not an appropriate or realistic estimate because the biosphere and accessible H_2 flux cannot be evenly distributed throughout the ocean. Instead, if present, methanogens will be isolated to the seafloor or subseafloor (Cable et al., 2021) in an uncertain habitable volume which is likely at least three orders of magnitude smaller than the bulk ocean (Ray et al., 2021). Cell densities could be much larger than those calculated above if the volume is

small, but they may also be smaller if the volume is large and at sufficiently high temperature (Figures 5c and 5d). In any case, currently unconstrained heterogeneities in the seafloor mean that quantifying an in situ biomass density is not trivial. Thankfully, many useful interpretations can be made using the total biomass and turnover alone.

Importantly, all arguments above rely on the a priori assumption that the proposed habitat is habitable. The likelihood of this, for the relevant distributions, is shown in Figure 5e. Despite the habitable parameter space at pH 9 predicting higher biomasses on average, their actual existence is less probable than at pH 8, as discussed in Section 3.1.

4. Discussion

Higgins et al. (2021) showed that despite the optimism around Enceladus' putative habitability, key gaps in the current understanding of its geophysics and geochemistry still leave significant uncertainties. Here, the habitable/uninhabitable classification is expanded to include a third criterion: energetically habitable but energy availability does not control the growth rate. This condition exists when plentiful energy for life exists, supporting exponential growth. However, critically, such a result could render the chemical composition, as derived by Cassini observations, unsustainable. Exponential growth almost always causes the ocean plume composition to change significantly and shift space plume gas ratios toward elevated [CH_4] and lower [H_2], as modeled by Higgins (2022), unless there are other limiting factors such as nutrient or heavy metal availability, toxicity, microbial competition, or spatial bioavailability. This could be akin to the "residual energy signature" suggested by Hoehler (2022).

In the habitable scenarios, distributions of biomass scale and total turnover (i.e., creation of new cellular carbon) as a function of biological H_2 consumption were estimated using a wide ocean parameter space. With this normalization, the biomass scale may span several orders of magnitude, but turnover can be more tightly constrained. Total scale and productivity were then determined as a function of the ratio between abiotic and biotic methane. In this section, the limitations of this approach are examined and its applications are explored. Section 4.1 discusses additional properties which may limit microbial growth on Enceladus. Section 4.2 examines the effect of elevated gas concentration near putative hydrothermal vents on this habitability interpretation. Sections 4.3 and 4.4 discuss and refine uncertainties in the presented biomass scale and turnover estimates. Section 4.5 explores whether there may be contradictions between the notional biosphere and other ongoing processes, and Section 4.6 describes the implications of this work in the context of life detection missions.

4.1. Nutrients, Toxicity, Metabolic, and Spatial Limitation

Critical nutrients such as iron and sulfur have not been directly detected without ambiguity on Enceladus, but their presence is expected (Cockell et al., 2021; Glein & Waite, 2020; Hao et al., 2022; Magee & Waite, 2017; Ray et al., 2021; Roche et al., 2023; Waite et al., 2017). Phosphorus was recently detected from Cassini E ring measurements (Postberg et al., 2023), and recent geochemical modeling analyses predict that it is unlikely to be a limiting nutrient (Hao et al., 2022; Randolph-Flagg et al., 2023). The effectiveness of microbial models to predict the cell-specific limiting effects of individual nutrients requires rigorous empirical study and key parameters are often unavailable (Higgins & Cockell, 2020). Toxicity of chemical species such as hydrogen cyanide (HCN) is highly organism-dependent and a complex habitability parameter to quantify, so it is rarely included in habitability models, although kinetic models describing how toxicity of some species affects the rate of microbial methanogenesis have been developed (e.g., Kim et al., 1994; Puyol et al., 2012). Recent analyses suggest that Enceladus plume material may contain a significant quantity of HCN (Peter et al., 2023) at mixing ratios corresponding to approximately half the concentration of CO_2(aq) (up to mM) if all detected HCN is present in the ocean. Such concentrations, which could contribute to prebiotic chemistry and have been suggested to play a role in the origin of life (Miyakawa et al., 2002), are toxic to many (but not all) life forms, particularly methanogens, because cyanides sequester vital metal ions (Luque-Almagro et al., 2018). Alternatively, a significant contribution of this HCN could be sourced from the ice shell rather than the ocean, and collected on the space plume during transit (Peter et al., 2023), possibly explaining the tentative detection of a C ≡ N signature on the surface (Villanueva et al., 2023). Further modeling is needed to elucidate the origins of the HCN and its effect on Enceladus' ocean toxicity. Competition with other microbes for metabolites or nutrients may also limit methanogen growth, but even when radiolytic production of alternative oxidants is considered, Ray et al. (2021)

concluded that hydrogenotrophic methanogenesis still appears to be the metabolism with the highest energy yield and biomass potential. If Enceladus is younger than once thought (Ćuk & Moutamid, 2023; Ćuk et al., 2016; though see also Nimmo et al., 2023) and/or life is in the early stages of evolution, metabolic inefficiencies may explain some of the high Gibbs free energies inferred. Finally, spatial constraints (e.g., restricted space for a habitat on the seafloor) could limit access to H_2 despite it being readily available in solution, particularly if the ocean plume is rotationally controlled and spatially isolated to a column during transit to the ice layer (e.g., Choblet et al., 2017; Schoenfeld et al., 2023), though wider mixing of seawater with HF and longer timescales of vertical transport have been proposed (e.g., Kang et al., 2022).

Any and all of the above factors could reduce the methanogen growth rate, steady state biomass and cell turnover rates predicted in this study, whether energy-limited or not. How these factors can be quantitatively incorporated into habitability and biomass estimates remains an open question. For nutrients, one could generate turnover distributions similar to those presented here to estimate the flux required of key nutrients and heavy metals (e.g., CHNOPS + TM; Cockell et al., 2021) to support the biosphere, or ideally model their production directly and incorporate those fluxes (e.g., for phosphorus: Hao et al., 2022; Randolph-Flagg et al., 2023). For toxicity and spatial factors, laboratory experiments could help constrain half-saturation constants for methanogenic growth in Enceladus-like conditions.

4.2. Increased Seawater/HF Mixing Boosts Likelihood of Habitability in a Highly Alkaline Ocean

The present results suggest that if Enceladus' bulk ocean pH is 7–8, alternative mechanisms to limit the scale of the biosphere must be involved. Importantly, this includes the null hypothesis, that is, there is no life present. Geochemical consensus continues to gravitate toward an ocean pH of 8–9 (e.g., Fifer et al., 2022; Glein & Waite, 2020). This work suggests this is indeed the most probable pH range to sustain an energy-limited methanogenic biosphere that does not significantly alter ocean chemistry as-observed to date. The situation is different when one considers the degree of mixing with HF that a purported methanogen habitat may have beyond that expected in the ocean plume. An endowment of up to 10 times the steady state [H_2(aq)] and [CH_4(aq)] may increase this energy-limited habitability window by up to one unit of bulk ocean pH. In other words, while the HSW of a pH 8–9 ocean may be energy-limited, regions with a higher contribution of HF and the associated elevated [H_2] and [CH_4], such as those in close proximity to hydrothermal vents, are less likely to be energy-limited. Therefore, a seafloor habitat like this, if inhabited, must be restricted by the alternative influences outlined above. Alternatively, if the ocean has a higher bulk ocean pH of around 9–10, the seafloor itself is more difficult (albeit not impossible) to survive in, but locations with elevated hydrothermal fluid contributions could comfortably support microbial growth (Figure S2 in Supporting Information S1) provided any associated salinity increases do not significantly impede the bioavailability of H_2. This 10x increase is a limited approximation, and the true difference between SW and HF may be very different, but these results show that an alkaline ocean deemed less habitable by Higgins et al. (2021), may yet be host to habitable HF.

Arguments above suggest that if a notional habitat at the bottom of Enceladus' ocean had an additional contribution of HF, it would possess a larger probability of energetic habitability than one containing only HSW. The inverse may be true at the top of the ocean, because the bioavailability of H_2 and to a lesser extent CO_2 is limited by their tendency to partially exsolve, particularly in the plume formation region. This exsolution is due to the lower pressure at the top of the ocean relative to the bottom. At ∼1 bar and 273K (approximating the ice-water boundary) the maximum bioavailable concentration of H_2 is ∼0.1 mmol kg^{-1}. If Enceladus seawater is more saline than the parameter space used here (e.g., Lobo et al., 2021) or more importantly if the ice shell is thin and permits lower pressures, bioavailability will be further reduced. This highlights the need for models to include pressure and exsolution as key parameters, particularly when critical habitability drivers are dissolved gases such as CO_2 and H_2.

More broadly, it is important to be aware that the understood parameter space of Enceladus' SW and HF is rapidly changing and updating through modeling (Fifer et al., 2022; Hsu et al., 2015; Kang et al., 2022; Lobo et al., 2021; Park et al., 2024), re-examining Cassini data (e.g., Peter et al., 2023; Postberg et al., 2023), and comparison to terrestrial analogs (e.g., Fukushi et al., 2020). The parameter space used here was broad and tried to capture conditions which fall within most current models to give an overview of Enceladus' possible habitability, biomass, and productivity. The HF and elevated salinity approximations show ways in which the MC model can be adjusted to accommodate this changing understanding as needed. For example, [DIC] on Enceladus may have

a larger upper limit endmember than the one included here (e.g., up to 0.2 mol kg^{-1} (Fukushi et al., 2020)), which may have a similar effect on the likelihoods of habitability conditions A, B, and C, and the associated biomass distributions as the HF approximation discussed above.

4.3. Uncertainties in Notional Steady State Biomass

This work constrained pH and temperature dependent probability distributions of steady state biomass and cell turnover rates in Enceladus' ocean using Cassini observations and geochemical modeling analyses. Extending habitability models to create these estimates required additional simplifications and assumptions, introducing a variety of ways in which such estimates could be revised up or down, with implications for biosignature research and the expected probability of life detection.

Biomass and cell turnover were constrained per mole of H_2 consumed per second. This distinction has important implications for how Figures 2–4 should be interpreted. While it appears at first glance that a cooler habitat can host a larger biomass, owing to lower maintenance powers and slower metabolic rates, this is an unlikely endmember of Enceladus's parameter space to host a large methanogenic biosphere because the bioavailable H_2 flux is most likely to be concentrated near its higher temperature source at or below the seafloor (Cable et al., 2021). Therefore, the notional methanogenic biomass and microbial consumption rate of H_2 is likely to be minimal in low temperature environments such as the ice-water boundary or saline microhabitats in the ice (should either be viable habitats) compared to subseafloor environments at higher temperatures. In actuality, no single homogeneous location would access all of the H_2 flux, but this work provides "building blocks" which capture the entire possible biomass range. A future, more rigorous analysis could consider a variety of habitats, each with a different distribution akin to those in Figure 3, and individual rates of biological H_2 consumption, building an interconnected notional Enceladus ecosystem. Biosignatures and their longevity could also be monitored in such a model.

With that in mind, the biomass calculations performed in this work can be compared to previous studies. In the unlikely 273 K, pH_{bo} 8, maximally biotic CH_4 endmember, a mean of 10^{23} cells could be supported on $\sim 10^3$ mol/s of H_2 flux, respectively (Figure 5c). In a more realistic elevated temperature habitat where $T > 350$K, this estimate becomes $<10^{20}$ cells for the pH 8 ocean (Figure 5c), or $<10^{21}$ cells for the pH 9 ocean (Figure 5d). At the lower endmember of biological H_2 consumption, 10 mol s^{-1}, the values for biomass above would be two orders of magnitude lower, that is, $<10^{18}$ cells when $pH_{bo} = 8$. While cell densities in cells cm^{-3} would provide a useful comparison to analog Earth environments, such a calculation is not trivial when the scale of the Enceladus habitat is not known. Although these are very general estimates (e.g., that the habitat is localized to a single T and pH_{bo}), the pH_{bo} 8, low J^{bio}_{H2}, 100% biotic CH_4 endmember is commensurate with the space plume informed biotic CH_4 posterior distribution of putative cells in a seafloor hydrothermal system predicted by the thermodynamic ecological model of Affholder et al. (2022), $10^{18\pm0.07}$. A more appropriate comparison which corrects for cell size is the total cellular carbon [kgC]. The methanogens simulated here have a carbon dry mass of 5×10^{-16} kgC $cell^{-1}$ (Higgins & Cockell, 2020), so the total kgC is the total cell count multiplied by this dry mass. The most probable plume-informed total standing biomass from Affholder et al. (2022) was $4–6 \times 10^3$ kgC, comparable to the results of the present study with minimal H_2 consumption (i.e., $<1 \times 10^3$ kgC at pH_{bo} 8 and $<5 \times 10^3$ kgC at pH_{bo} 9 both with $T > 350$ K). Confidence intervals for these notional biomasses are noted in Tables S8 and S12 of the Supporting Information S1. Consequently, this parameter space can present either lower or higher total standing biomasses but is in broad agreement with Affholder et al. (2022) in that an Enceladus methanogen biosphere, if it exists, is likely small. Total biomass will scale with biological H_2 consumption provided the habitats have sufficient nutrient availability. However, to remain conservative, consistent with other literature estimates, and vigilant for possible false negative life detection observations, the biomass at 10 mol s^{-1} H_2 consumption ($<10^{18}$ cells, $<10^3$ kgC when $pH_{bo} = 8$; $<10^{19}$ cells, $<10^{3.7}$ kgC when $pH_{bo} = 9$) sets a good benchmark for Enceladus' notional methanogenic biosphere.

4.4. Uncertainties in Notional Cell Turnover

Cellular turnover rate is inversely proportional to the energetic cost of biomass synthesis at first order because it determines how many cells can be generated using a given power available for growth. In NutMEG, this growth power is what remains of the power supply after considering maintenance requirements and nutrient limitation (Higgins & Cockell, 2020). The present Enceladus biomass turnover model used a theoretical minimum biomass synthesis requirement, whereas global turnover predictions were corrected by an order of magnitude decrease,

better reflecting what is expected in natural systems (McCollom & Amend, 2005; Figure 5b). This identifies the energetic cost of biosynthesis as a key variable in biosphere and turnover characterization, with its explicit effect on productivity shown in Figure 5b. Therefore, improving constraints on this parameter and its variation with different physicochemical environments has the potential to refine biomass and turnover estimates by orders of magnitude.

The total notional Enceladean cell turnover per mole of H_2 consumed is more tightly constrained than the corresponding steady state biomass and lies within bounds of approximately one order of magnitude, less the uncertainty in synthesis energy noted above. In the limit that all plume methane is biotic, this range of 10^4–10^6 kg C yr^{-1} is broadly in agreement with the similarly maximally biotic CH_4 ranges predicted by Affholder et al. (2022) (plume-informed posterior distribution between 3×10^5 and 4×10^6 kgC yr^{-1}) and Steel et al. (2017) (4×10^4–2×10^6 kgC yr^{-1}), though slightly lower which could be caused by this work's inclusion of a dynamic turnover rate. These estimates should be considered upper limits, because methane can also be produced abiotically. The range from this work can be more tightly constrained by isolating a notional habitat to a specific temperature or pH window (Figure 3, Tables S2–S26 in Supporting Information S1). Cellular carbon turnover is estimated here to be of order mg C per kg flux of the ocean plume (Figure 5b). This is comparable to the total productivity in Earth hydrothermal plumes (up to 50 mg kg^{-1}, where methanogenesis is a minor contributor at 1.9 mg kg^{-1} (McCollom, 2000)). Competition for H_2 with other biological species could lower this estimate of Enceladus' notional methanogen biomass and turnover, as discussed in Section 4.6.

4.5. Extant Biosphere May Not Contradict Existing Observations and Inferring Its Scale Requires Abiotic/Biotic Carbon Measurements

One proposed source of H_2 on Enceladus could be rock-alteration processes such as serpentinization, but modeled H_2 generation rates vary by several orders of magnitude (Cable et al., 2020; Daval et al., 2022; Glein & Waite, 2020; Glein et al., 2018; Steel et al., 2017; Taubner et al., 2018; Vance et al., 2016; Waite et al., 2017; Zandanel et al., 2021). Many estimates do not reach the rates required to explain the observed flux of space plume H_2 (Figure S4 in Supporting Information S1). Daval et al. (2022) suggest that serpentinization may only be able to last on Enceladus for ∼10 Myr. Other mechanisms, such as radiolysis (Bouquet et al., 2017; Ray et al., 2021), or yet-unknown processes may contribute to ongoing H_2 production on Enceladus. Figure 5a reveals that the total H_2 generation required to be consistent with plume observations is not significantly altered by the existence of a methanogenic biosphere. This finding is important as it demonstrates that within the uncertainty of the space plume composition and fluxes, total H_2 production from radiolysis, serpentinization and other processes is independent of the ratio of abiotic/biotic methane, and the difficulty of putting any constraints on that ratio at this point in time. Here, abiotic H_2 and CH_4 production were decoupled (e.g., not presuming any single geochemical explanation for the source of the abiotic methane). This is reasonable because the required H_2 production in Figure 5a does not change significantly in the context of its uncertainty between $10^{-6} < R_{ab:b} < 10^6$ (staying well within the range of $10^{1.4}$–$10^{3.2}$ mol s^{-1} as seen on the vertical axis of Figure 5a). Even if each molecule of CH_4 produced abiotically consumes 4 H_2, the total required H_2 production remains close to the range shown in Figure 5a. In a more general sense, this means that the H_2 to CH_4 ratio in the space plume alone can neither inform the abiotic to biotic CH_4 ratio nor the scale of the notional biosphere. In contrast, if it were possible to estimate the abiotic to biotic CH_4 or organic molecule ratio, for example, through measurement of carbon isotope fractionation or chirality, then the possible scale of the biosphere and probability of life detection could be constrained further.

Consequently, measurement of $\delta^{13}C$ in CO_2 and CH_4 may place a fixed window of biomass scale and productivity on Enceladus and other icy moons. Figure 5b shows how notional biosphere productivity can be linked to the biotic contribution to space plume methane. Assessing $R_{ab:b}$ through isotopic observations and careful consideration of the possible abiotic sources (e.g., isotope fractionation between methane and higher order hydrocarbons; (Sherwood Lollar et al., 2002)) may help further constrain the possible scale and biotic carbon production of Enceladus' biosphere, if it exists. In advance of and alongside these anticipated observations, thorough modeling analyses that constrain the isotopic signature of the possible abiotic and biotic processes should be performed. These will help interpret the data as reliably as possible. A similar ratio to corroborate that estimate could be the ratio of abiotic to biotic organic material, constrained through $\delta^{13}C$ or chirality measurements. Such measurements should be of critical importance when proposing space missions with science goals including life detection (MacKenzie et al., 2021; Seaton et al., 2023). This approach can be extended to other icy moons such as Europa or Titan. The neutral gas mass spectrometer aboard Europa Clipper may be able to measure the isotopic composition

of volatiles (Brockwell et al., 2016; Chou et al., 2021), so an approach like the one presented here could help inform the scale of a notional biosphere on Europa.

4.6. Prospects for a More Diverse Biosphere and Life Detection

This study focused on Enceladus' notional methanogenic biosphere, but methanogenesis may not be the only metabolism that Enceladus can host, and several other candidates have been proposed (e.g., Ray et al., 2021; Roche et al., 2023; Yanez et al., 2024). Other biological species could affect notional methanogen growth. For example, competition with sulfate reducers for H_2 may reduce their viability, or syntrophy with fermenting bacteria could boost their growth. The total biomass stock could also increase as more diverse energy sources are utilized beyond CO_2 and H_2. Additional biological species will also affect the amount of cell turnover (based on population size) and perhaps the amount of necromass which is delivered to the space plume, for example, through heterotrophy. However, ecosystem modeling of such complexity is beyond the scope of what can feasibly be done for Enceladus at present. This would require better resolved geochemical models of redox flux and better spatial understanding of Enceladus' possible habitats.

Abiotic mechanisms which dilute or concentrate biomass and necromass may also occur at multiple stages through transit from the notional habitat to the space plume and/or Enceladus' surface and are discussed by Affholder et al. (2022). Although amino acids are expected to persist in Enceladus' bulk ocean for long timescales (Truong et al., 2019), they may decompose if residence time in a hot habitat is too long. Significant dilution of the hydrothermal mixing column into the wider ocean may be possible (e.g., Kang et al., 2022) but may not be important if the ocean plume conserves its angular momentum to the ice layer (Choblet et al., 2017; Schoenfeld et al., 2023). However, both residence timescales and concentration/dilution of organic matter when traveling from the ice/water boundary into the space plume remain open questions. Biotic carbon may also be altered by ionizing radiation, fractionated via interaction with the ice wall, or concentrated via "bubble scrubbing." In this process, gas bubbles disturb an organic-rich layer at the top of the water table as they burst when emerging from the ocean, liberating some of the organic matter in the process (Porco et al., 2017). Water vapor then condenses around the bubbles forming organic-rich ice grains, a fraction of which "snow" onto Enceladus' surface (Porco et al., 2017; Postberg et al., 2018). Recent experiments suggest that these grains may be able to entrain cells (Perera & Cockell, 2023).

If the biotic carbon is predominantly captured in ice grains which are ejected into the plume, then the milligrams of biotic carbon per kg of H_2O estimate shown in Figure 5b could be a conservative underestimate of their concentration in ice grains. The total water flux of 100–1,000 kg H_2O s^{-1} is dominated by water vapor, with a much lower fraction of that mass (of order 10s kg s^{-1}) expected to be ice grains (Cable et al., 2020; Porco et al., 2017; Southworth et al., 2019). Only a subset of Type II ice grains have been identified as organic-rich, with up to 1% by mass organic carbon content (Postberg et al., 2018). If Enceladus is inhabited and *all* cellular carbon turnover is introduced into the plume ice grains, up to order grams of biotic carbon could be expected per kg ice grains and hence be an important contributor to the total organic content. Development of methods evaluating abiotic to biotic ratios of complex organic material as well as methane (e.g., stable isotopes or chirality) will therefore be important in the coming years to supplement life detection missions.

Affholder et al. (2022) describe a technique to estimate the number of flybys required by the concept Enceladus Orbilander spacecraft (MacKenzie et al., 2021) to reach 95% confidence that a cell is observed. They estimate that approximately 100 low plume fly throughs (totaling 0.1 mL) are required to alleviate the risk of only collecting false negative samples, if there is no bubble scrubbing. As the biomass turnover predicted in this work and by Steel et al. (2017) are comparable to those of Affholder et al. (2022), this detection limit should act as a good benchmark for Enceladus. As noted above, however, model assumptions can cause turnover estimates to vary by several orders of magnitude, and order of magnitude differences in the required number of plume fly throughs can have important implications on the feasibility of ruling out false negatives.

5. Conclusions

The probability of habitability across the expected parameter space of Enceladus was determined along with the H_2-limited biomass and cell turnover rates which may exist in its habitable space. If the bulk ocean pH is 8–9 as expected, there is 40%–60% probability that a notional methanogen biosphere would be energy limited. Alternatively, this range could also reflect uninhabitable conditions, or conditions where energy is not the microbial

growth limiting step. The biosphere Enceladus could sustain is commensurate with other estimates within a broad distribution of possibilities, and the mean expected biomass of a 350 K seafloor habitat is 10^3, $10^{3.7}$ kgC ($\sim 10^{18}$, 10^{19} cells) with ocean-top pH 8, 9, respectively, if total microbial H_2 consumption is 10 mol s^{-1}. However, mean values like this are limited estimates and the possibilities span several orders of magnitude. The biosphere size also scales linearly with its H_2 consumption. Cell turnover is more tightly constrained, and the rate of production of biotic carbon in any ocean habitat is $\sim 10^4$–10^6 kgC per year provided >50% of the methane observed in the space plume was biotic. This is useful because cell turnover is a critical parameter to constrain for life detection missions; it directly influences how much biomass is being created and how much of that might reach the space plume and be detectable. In situ cell density cannot be estimated until more is known about the scale of the putative habitat(s).

As models and experiments continue to quantify mechanisms of cell and organic matter transit from the ocean to deposition on Enceladus' surface, they can be combined with this turnover model to estimate the cell concentrations which may be encountered by future spacecraft such as the concept Enceladus Orbilander. In the case where it is not feasible to sample at the surface or where cell counts are expected to be below detection limits, measurements of isotopic fractionation in elements such as carbon and the chirality of organics may help further constrain the abiotic to biotic ratios of astrobiologically relevant chemical species and, in turn, the biomass estimates presented in this work and by others.

Data Availability Statement

The source code for NutMEG and links to its documentation are available in the NutMEG github repository: https://github.com/pmhiggins/NutMEG and archived in Zenodo (Higgins, 2024a). For this study, version 1.0.1 was used. The code required to replicate these results is available in the NutMEG-Implementations GitHub repository in the EnceladusBiomassBiosignatures directory: https://github.com/pmhiggins/NutMEG-Implementations/ (also archived in Zenodo, (Higgins, 2024b)). Data sets generated for this work are archived on figshare (Higgins et al., 2024). A glossary of symbols and units is available in Table S1 of the Supporting Information S1. Supporting Text, Tables, and Figures are available in Supporting Information S1.

Acknowledgments
This study was financially supported by the Natural Sciences and Engineering Research Council of Canada Discovery and New Frontiers in Research Fund grants to BSL. Early developments in this work were supported by a Science and Technology Facilities Council (STFC) scholarship to PMH. BSL is a Director of the CIFAR Earth 4D Subsurface Science and Exploration program. The authors thank Oliver Warr (U. Ottawa) for constructive conversations, and two anonymous reviewers for their constructive comments.

References

Affholder, A., Guyot, F., Sauterey, B., Ferrière, R., & Mazevet, S. (2021). Bayesian analysis of Enceladus's plume data to assess methanogenesis. *Nature Astronomy*, *5*(8), 1–10. https://doi.org/10.1038/s41550-021-01372-6

Affholder, A., Guyot, F., Sauterey, B., Ferrière, R., & Mazevet, S. (2022). Putative methanogenic biosphere in Enceladus's deep ocean: Biomass, productivity, and implications for detection. *The Planetary Science Journal*, *3*(12), 270. https://doi.org/10.3847/PSJ/aca275

Bouquet, A., Glein, C. R., Wyrick, D., & Waite, J. H. (2017). Alternative energy: Production of H_2 by radiolysis of water in the rocky cores of icy bodies. *The Astrophysical Journal*, *840*(1), L8. https://doi.org/10.3847/2041-8213/aa6d56

Brockwell, T. G., Meech, K. J., Pickens, K., Waite, J. H., Miller, G., Roberts, J., et al. (2016). The mass spectrometer for planetary exploration (MASPEX). In *2016 IEEE aerospace conference* (pp. 1–17). Big Sky, IEEE. https://doi.org/10.1109/AERO.2016.7500777

Buan, N. R. (2018). Methanogens: Pushing the boundaries of biology. *Emerging Topics in Life Sciences*, *2*(4), 629–646. https://doi.org/10.1042/ETLS20180031

Cable, M. L., Neveu, M., Hsu, H.-W., & Hoehler, T. M. (2020). Enceladus. In V. S. Meadows, D. J. Des Marais, G. N. Arney, & B. E. Schmidt (Eds.), *Planetary astrobiology* (pp. 217–246). University of Arizona Press.

Cable, M. L., Porco, C., Glein, C. R., German, C. R., MacKenzie, S. M., Neveu, M., et al. (2021). The science case for a return to Enceladus. *The Planetary Science Journal*, *2*(4), 132. https://doi.org/10.3847/PSJ/abfb7a

Choblet, G., Tobie, G., Sotin, C., Běhounková, M., Čadek, O., Postberg, F., & Souček, O. (2017). Powering prolonged hydrothermal activity inside Enceladus. *Nature Astronomy*, *1*(12), 841–847. https://doi.org/10.1038/s41550-017-0289-8

Chou, L., Mahaffy, P., Trainer, M., Eigenbrode, J., Arevalo, R., Brinckerhoff, W., et al. (2021). Planetary mass spectrometry for agnostic life detection in the solar system. *Frontiers in Astronomy and Space Sciences*, *8*, 755100. https://doi.org/10.3389/fspas.2021.755100

Cockell, C. S., Simons, M., Castillo-Rogez, J., Higgins, P. M., Kaltenegger, L., Keane, J. T., et al. (2024). Sustained and comparative habitability beyond Earth. *Nature Astronomy*, *8*(1), 30–38. https://doi.org/10.1038/s41550-023-02158-8

Cockell, C. S., Stevens, A. H., & Prescott, R. (2019). Habitability is a binary property. *Nature Astronomy*, *3*(11), 956–957. https://doi.org/10.1038/s41550-019-0916-7

Cockell, C. S., Wordsworth, R., Whiteford, N., & Higgins, P. M. (2021). Minimum units of habitability and their abundance in the universe. *Astrobiology*, *21*(4), 481–489. https://doi.org/10.1089/ast.2020.2350

Ćuk, M., Dones, L., & Nesvorný, D. (2016). Dynamical evidence for a late formation of Saturn's moons. *The Astrophysical Journal*, *820*(2), 97. https://doi.org/10.3847/0004-637X/820/2/97

Ćuk, M., & Moutamid, M. E. (2023). A past episode of rapid tidal evolution of Enceladus? *The Planetary Science Journal*, *4*(7), 119. https://doi.org/10.3847/PSJ/acde80

Daval, D., Choblet, G., Sotin, C., & Guyot, F. (2022). Theoretical considerations on the characteristic timescales of hydrogen generation by serpentinization reactions on Enceladus. *Journal of Geophysical Research: Planets*, *127*(2), e2021JE006995. https://doi.org/10.1029/2021JE006995

Etiope, G., & Sherwood Lollar, B. (2013). Abiotic methane on Earth. *Reviews of Geophysics*, *51*(2), 276–299. https://doi.org/10.1002/rog.20011

Fifer, L. M., Catling, D. C., & Toner, J. D. (2022). Chemical fractionation modeling of plumes indicates a gas-rich, moderately alkaline Enceladus ocean. *The Planetary Science Journal*, *3*(8), 191. https://doi.org/10.3847/PSJ/ac7a9f

Fukushi, K., Imai, E., Sekine, Y., Kitajima, T., Gankhurel, B., Davaasuren, D., & Hasebe, N. (2020). In situ formation of monohydrocalcite in alkaline saline lakes of the valley of Gobi Lakes: Prediction for Mg, Ca, and total dissolved carbonate concentrations in Enceladus' ocean and alkaline-carbonate ocean worlds. *Minerals*, *10*(8), 669. https://doi.org/10.3390/min10080669

Glein, C. R., Baross, J. A., & Waite, J. H. (2015). The pH of Enceladus' ocean. *Geochimica et Cosmochimica Acta*, *162*, 202–219. https://doi.org/10.1016/j.gca.2015.04.017

Glein, C. R., Postberg, F., & Vance, S. D. (2018). The geochemistry of Enceladus: Composition and controls. In P. M. Schenk, R. N. Clark, C. J. A. Howett, A. J. Verbiscer, & J. H. Waite (Eds.), *Enceladus and the icy Moons of Saturn* (pp. 39–56). University of Arizona Press. https://doi.org/10.2458/azu_uapress_9780816537075-ch003

Glein, C. R., & Waite, J. H. (2020). The carbonate geochemistry of Enceladus' ocean. *Geophysical Research Letters*, *47*(3), e2019GL085885. https://doi.org/10.1029/2019GL085885

Hansen, C. J., Shemansky, D. E., Esposito, L. W., Stewart, A. I. F., Lewis, B. R., Colwell, J. E., et al. (2011). The composition and structure of the Enceladus plume. *Geophysical Research Letters*, *38*(11), L11202. https://doi.org/10.1029/2011GL047415

Hao, J., Glein, C. R., Huang, F., Yee, N., Catling, D. C., Postberg, F., et al. (2022). Abundant phosphorus expected for possible life in Enceladus's ocean. *Proceedings of the National Academy of Sciences of the United States of America*, *119*(39), e2201388119. https://doi.org/10.1073/pnas.2201388119

Harvie, C. E., Møller, N., & Weare, J. H. (1984). The prediction of mineral solubilities in natural waters: The Na-K-Mg-Ca-H-Cl-SO_4-OH-HCO_3-CO_3-CO_2-H_2O system to high ionic strengths at 25°C. *Geochimica et Cosmochimica Acta*, *48*(4), 723–751. https://doi.org/10.1016/0016-7037(84)90098-X

Helgeson, H. C., Kirkham, D. H., & Flowers, G. C. (1981). Theoretical prediction of the thermodynamic behavior of aqueous electrolytes by high pressures and temperatures; IV, Calculation of activity coefficients, osmotic coefficients, and apparent molal and standard and relative partial molal properties to 600°C and 5kb. *American Journal of Science*, *281*(10), 1249–1516. https://doi.org/10.2475/ajs.281.10.1249

Hendrix, A. R., Hurford, T. A., Barge, L. M., Bland, M. T., Bowman, J. S., Brinckerhoff, W., et al. (2018). The NASA roadmap to ocean worlds. *Astrobiology*, *19*(1), 1–27. https://doi.org/10.1089/ast.2018.1955

Higgins, P. M. (2022). Modelling extraterrestrial habitability, biomass and biosignatures through the bioenergetic lens. (Doctoral). The University of Edinburgh.

Higgins, P. M. (2024a). pmhiggins/NutMEG: Enceladus and TOM compatability update (version v1.0.1) [Software]. *Zenodo*. https://doi.org/10.5281/zenodo.10647796

Higgins, P. M. (2024b). pmhiggins/NutMEG-Implementations: Enceladus biomass and biotic carbon turnover (version v1.1.0) [Software]. *Zenodo*. https://doi.org/10.5281/zenodo.10647803

Higgins, P. M., Chen, W., Glein, C. R., Cockell, C. S., & Sherwood Lollar, B. (2024). Supplemental data for "Quantifying uncertainty in sustainable biomass and production of biotic carbon in Enceladus' notional methanogenic biosphere" (version 2) [Dataset]. *figshare*. https://doi.org/10.6084/m9.figshare.22557706.v2

Higgins, P. M., & Cockell, C. S. (2020). A bioenergetic model to predict habitability, biomass and biosignatures in astrobiology and extreme conditions. *Journal of the Royal Society Interface*, *17*(171), 20200588. https://doi.org/10.1098/rsif.2020.0588

Higgins, P. M., Glein, C. R., & Cockell, C. S. (2021). Instantaneous habitable windows in the parameter space of Enceladus' ocean. *Journal of Geophysical Research: Planets*, *126*(11), e2021JE006951. https://doi.org/10.1029/2021JE006951

Hoehler, T. M. (2007). An energy balance concept for habitability. *Astrobiology*, *7*(6), 824–838. https://doi.org/10.1089/ast.2006.0095

Hoehler, T. M. (2022). Implications of H_2/CO_2 disequilibrium for life on Enceladus. *Nature Astronomy*, *6*(1), 3–4. https://doi.org/10.1038/s41550-021-01583-x

Hsu, H.-W., Postberg, F., Sekine, Y., Shibuya, T., Kempf, S., Horányi, M., et al. (2015). Ongoing hydrothermal activities within Enceladus. *Nature*, *519*(7542), 207–210. https://doi.org/10.1038/nature14262

Iess, L., Stevenson, D. J., Parisi, M., Hemingway, D., Jacobson, R. A., Lunine, J. I., et al. (2014). The gravity field and interior structure of Enceladus. *Science*, *344*(6179), 78–80. https://doi.org/10.1126/science.1250551

Jin, Q., & Bethke, C. M. (2007). The thermodynamics and kinetics of microbial metabolism. *American Journal of Science*, *307*(4), 643–677. https://doi.org/10.2475/04.2007.01

Johnson, J. W., Oelkers, E. H., & Helgeson, H. C. (1992). SUPCRT92: A software package for calculating the standard molal thermodynamic properties of minerals, gases, aqueous species, and reactions from 1 to 5000 bar and 0 to 1000 C. *Computers & Geosciences*, *18*(7), 899–947. https://doi.org/10.1016/0098-3004(92)90029-Q

Kang, W., Marshall, J., Mittal, T., & Bire, S. (2022). Ocean dynamics and tracer transport over the south pole geysers of Enceladus. *Monthly Notices of the Royal Astronomical Society*, *517*(3), 3485–3494. https://doi.org/10.1093/mnras/stac2882

Khawaja, N., Postberg, F., Hillier, J., Klenner, F., Kempf, S., Nölle, L., et al. (2019). Low-mass nitrogen-oxygen-bearing, and aromatic compounds in Enceladean ice grains. *Monthly Notices of the Royal Astronomical Society*, *489*(4), 5231–5243. https://doi.org/10.1093/mnras/stz2280

Kim, I. S., Young, J. C., & Tabak, H. H. (1994). Kinetics of acetogenesis and methanogenesis in anaerobic reactions under toxic conditions. *Water Environment Research*, *66*(2), 119–132. https://doi.org/10.2175/WER.66.2.5

Leal, A. M. M. (2015). Reaktoro: An open-source unified framework for modeling chemically reactive systems. Retrieved from https://reaktoro.org

Lever, M. A., Rogers, K. L., Lloyd, K. G., Overmann, J., Schink, B., Thauer, R. K., et al. (2015). Life under extreme energy limitation: A synthesis of laboratory- and field-based investigations. *FEMS Microbiology Reviews*, *39*(5), 688–728. https://doi.org/10.1093/femsre/fuv020

Lobo, A. H., Thompson, A. F., Vance, S. D., & Tharimena, S. (2021). A pole-to-equator ocean overturning circulation on Enceladus. *Nature Geoscience*, *14*(4), 185–189. https://doi.org/10.1038/s41561-021-00706-3

Luque-Almagro, V. M., Cabello, P., Sáez, L. P., Olaya-Abril, A., Moreno-Vivián, C., & Roldán, M. D. (2018). Exploring anaerobic environments for cyanide and cyano-derivatives microbial degradation. *Applied Microbiology and Biotechnology*, *102*(3), 1067–1074. https://doi.org/10.1007/s00253-017-8678-6

MacKenzie, S. M., Neveu, M., Davila, A. F., Lunine, J. I., Craft, K. L., Cable, M. L., et al. (2021). The Enceladus orbilander mission concept: Balancing return and resources in the search for life. *The Planetary Science Journal*, *2*(2), 77. https://doi.org/10.3847/PSJ/abe4da

Magee, B. A., & Waite, J. H. (2017). Neutral gas composition of Enceladus' plume—Model parameter insights from Cassini-INMS. In *Presented at the lunar and planetary science conference*.

McCollom, T. M. (2000). Geochemical constraints on primary productivity in submarine hydrothermal vent plumes. *Deep Sea Research Part I: Oceanographic Research Papers*, *47*(1), 85–101. https://doi.org/10.1016/S0967-0637(99)00048-5

McCollom, T. M., & Amend, J. P. (2005). A thermodynamic assessment of energy requirements for biomass synthesis by chemolithoautotrophic micro-organisms in oxic and anoxic environments. *Geobiology*, *3*(2), 135–144. https://doi.org/10.1111/j.1472-4669.2005.00045.x

Michał, B., Gagat, P., Jabłoński, S., Chilimoniuk, J., Gaworski, M., Mackiewicz, P., & Marcin, L. (2018). PhyMet2: A database and toolkit for phylogenetic and metabolic analyses of methanogens. *Environmental Microbiology Reports*, *10*(3), 378–382. https://doi.org/10.1111/1758-2229.12648

Miyakawa, S., Cleaves, H. J., & Miller, S. L. (2002). The cold origin of life: B. Implications based on pyrimidines and purines produced from frozen ammonium cyanide solutions. *Origins of Life and Evolution of the Biosphere*, *32*(3), 209–218. https://doi.org/10.1023/A:1019514022822

NASEM. (2022). *Origins, worlds, and life: A decadal strategy for planetary science and astrobiology 2023-2032*. National Academies Press. https://doi.org/10.17226/26522

Nimmo, F., Neveu, M., & Howett, C. (2023). Origin and evolution of Enceladus's tidal dissipation. *Space Science Reviews*, *219*(7), 57. https://doi.org/10.1007/s11214-023-01007-4

Park, R. S., Mastrodemos, N., Jacobson, R. A., Berne, A., Vaughan, A. T., Hemingway, D. J., et al. (2024). The global shape, gravity field, and libration of Enceladus. *Journal of Geophysical Research: Planets*, *129*(1), e2023JE008054. https://doi.org/10.1029/2023JE008054

Perera, L. J., & Cockell, C. S. (2023). Dispersion of bacteria by low-pressure boiling: Life detection in Enceladus' plume material. *Astrobiology*, *23*(3), 269–279. https://doi.org/10.1089/ast.2022.0009

Peter, J. S., Nordheim, T. A., & Hand, K. P. (2023). Detection of HCN and diverse redox chemistry in the plume of Enceladus. *Nature Astronomy*, *8*(2), 1–10. https://doi.org/10.1038/s41550-023-02160-0

Porco, C. C., Dones, L., & Mitchell, C. (2017). Could it be snowing microbes on Enceladus? Assessing conditions in its plume and implications for future missions. *Astrobiology*, *17*(9), 876–901. https://doi.org/10.1089/ast.2017.1665

Porco, C. C., Helfenstein, P., Thomas, P. C., Ingersoll, A. P., Wisdom, J., West, R., et al. (2006). Cassini observes the active south pole of Enceladus. *Science*, *311*(5766), 1393–1401. https://doi.org/10.1126/science.1123013

Postberg, F., Kempf, S., Schmidt, J., Brilliantov, N., Beinsen, A., Abel, B., et al. (2009). Sodium salts in E-ring ice grains from an ocean below the surface of Enceladus. *Nature*, *459*(7250), 1098–1101. https://doi.org/10.1038/nature08046

Postberg, F., Khawaja, N., Abel, B., Choblet, G., Glein, C. R., Gudipati, M. S., et al. (2018). Macromolecular organic compounds from the depths of Enceladus. *Nature*, *558*(7711), 564–568. https://doi.org/10.1038/s41586-018-0246-4

Postberg, F., Sekine, Y., Klenner, F., Glein, C. R., Zou, Z., Abel, B., et al. (2023). Detection of phosphates originating from Enceladus's ocean. *Nature*, *618*(7965), 489–493. https://doi.org/10.1038/s41586-023-05987-9

Puyol, D., Sanz, J. L., Rodriguez, J. J., & Mohedano, A. F. (2012). Inhibition of methanogenesis by chlorophenols: A kinetic approach. *New Biotechnology*, *30*(1), 51–61. https://doi.org/10.1016/j.nbt.2012.07.011

Randolph-Flagg, N. G., Ely, T., Som, S. M., Shock, E. L., German, C. R., & Hoehler, T. M. (2023). Phosphate availability and implications for life on ocean worlds. *Nature Communications*, *14*(1), 2388. https://doi.org/10.1038/s41467-023-37770-9

Ray, C., Glein, C. R., Hunter Waite, J., Teolis, B., Hoehler, T., Huber, J., et al. (2021). Oxidation processes diversify the metabolic menu on Enceladus. *Icarus*, *114248*, 114248. https://doi.org/10.1016/j.icarus.2020.114248

Roche, M. J., Fox-Powell, M. G., Hamp, R. E., & Byrne, J. M. (2023). Iron reduction as a viable metabolic pathway in Enceladus' ocean. *International Journal of Astrobiology*, *22*(5), 1–20. https://doi.org/10.1017/S1473550423000125

Schoenfeld, A. M., Hawkins, E. K., Soderlund, K. M., Vance, S. D., Leonard, E., & Yin, A. (2023). Particle entrainment and rotating convection in Enceladus' ocean. *Communications Earth & Environment*, *4*(1), 28. https://doi.org/10.1038/s43247-023-00674-z

Schönheit, P., Moll, J., & Thauer, R. K. (1980). Growth parameters (K s, μmax, Y s) of Methanobacterium thermoautotrophicum. *Archives of Microbiology*, *127*(1), 59–65. https://doi.org/10.1007/BF00414356

Seaton, K. M., Gyalay, S., de Quay, G. S., Burnett, E. R., Denton, C. A., Doerr, B., et al. (2023). Astrobiology eXploration at Enceladus (AXE): A new Frontiers mission concept study. *The Planetary Science Journal*, *4*(6), 116. https://doi.org/10.3847/PSJ/acd119

Sherwood Lollar, B., Lacrampe-Couloume, G., Voglesonger, K., Onstott, T. C., Pratt, L. M., & Slater, G. F. (2008). Isotopic signatures of CH_4 and higher hydrocarbon gases from Precambrian Shield sites: A model for abiogenic polymerization of hydrocarbons. *Geochimica et Cosmochimica Acta*, *72*(19), 4778–4795. https://doi.org/10.1016/j.gca.2008.07.004

Sherwood Lollar, B., Westgate, T. D., Ward, J. A., Slater, G. F., & Lacrampe-Couloume, G. (2002). Abiogenic formation of alkanes in the Earth's crust as a minor source for global hydrocarbon reservoirs. *Nature*, *416*(6880), 522–524. https://doi.org/10.1038/416522a

Smith, H. B., Drew, A., Malloy, J. F., & Walker, S. I. (2020). Seeding biochemistry on other worlds: Enceladus as a case study. *Astrobiology*, *21*(2), 177–190. https://doi.org/10.1089/ast.2019.2197

Southworth, B. S., Kempf, S., & Spitale, J. (2019). Surface deposition of the Enceladus plume and the zenith angle of emissions. *Icarus*, *319*, 33–42. https://doi.org/10.1016/j.icarus.2018.08.024

Steel, E. L., Davila, A., & McKay, C. P. (2017). Abiotic and biotic formation of amino acids in the Enceladus ocean. *Astrobiology*, *17*(9), 862–875. https://doi.org/10.1089/ast.2017.1673

Takai, K., Nakamura, K., Toki, T., Tsunogai, U., Miyazaki, M., Miyazaki, J., et al. (2008). Cell proliferation at 122°C and isotopically heavy CH_4 production by a hyperthermophilic methanogen under high-pressure cultivation. *Proceedings of the National Academy of Sciences of the United States of America*, *105*(31), 10949–10954. https://doi.org/10.1073/pnas.0712334105

Tanger, J. C., & Helgeson, H. C. (1988). Calculation of the thermodynamic and transport properties of aqueous species at high pressures and temperatures; revised equations of state for the standard partial molal properties of ions and electrolytes. *American Journal of Science*, *288*(1), 19–98. https://doi.org/10.2475/ajs.288.1.19

Taubner, R.-S., Pappenreiter, P., Zwicker, J., Smrzka, D., Pruckner, C., Kolar, P., et al. (2018). Biological methane production under putative Enceladus-like conditions. *Nature Communications*, *9*(1), 748. https://doi.org/10.1038/s41467-018-02876-y

Teolis, B. D., Perry, M. E., Hansen, C. J., Waite, J. H., Porco, C. C., Spencer, J. R., & Howett, C. J. A. (2017). Enceladus plume structure and time variability: Comparison of Cassini observations. *Astrobiology*, *17*(9), 926–940. https://doi.org/10.1089/ast.2017.1647

Thomas, P. C., Tajeddine, R., Tiscareno, M. S., Burns, J. A., Joseph, J., Loredo, T. J., et al. (2016). Enceladus's measured physical libration requires a global subsurface ocean. *Icarus*, *264*, 37–47. https://doi.org/10.1016/j.icarus.2015.08.037

Truong, N., Monroe, A. A., Glein, C. R., Anbar, A. D., & Lunine, J. I. (2019). Decomposition of amino acids in water with application to in-situ measurements of Enceladus, Europa and other hydrothermally active icy ocean worlds. *Icarus*, *329*, 140–147. https://doi.org/10.1016/j.icarus.2019.04.009

Vance, S. D., Hand, K. P., & Pappalardo, R. T. (2016). Geophysical controls of chemical disequilibria in Europa. *Geophysical Research Letters*, *43*(10), 4871–4879. https://doi.org/10.1002/2016GL068547

Villanueva, G. L., Hammel, H. B., Milam, S. N., Kofman, V., Faggi, S., Glein, C. R., et al. (2023). JWST molecular mapping and characterization of Enceladus' water plume feeding its torus. *Nature Astronomy*, *7*(9), 1056–1062. https://doi.org/10.1038/s41550-023-02009-6

Waite, J. H., Glein, C. R., Perryman, R. S., Teolis, B. D., Magee, B. A., Miller, G., et al. (2017). Cassini finds molecular hydrogen in the Enceladus plume: Evidence for hydrothermal processes. *Science*, *356*(6334), 155–159. https://doi.org/10.1126/science.aai8703

Waite, J. H., Lewis, W. S., Magee, B. A., Lunine, J. I., McKinnon, W. B., Glein, C. R., et al. (2009). Liquid water on Enceladus from observations of ammonia and ^{40}Ar in the plume. *Nature*, *460*(7254), 487–490. https://doi.org/10.1038/nature08153

Warr, O., Young, E. D., Giunta, T., Kohl, I. E., Ash, J. L., & Sherwood Lollar, B. (2021). High-resolution, long-term isotopic and isotopologue variation identifies the sources and sinks of methane in a deep subsurface carbon cycle. *Geochimica et Cosmochimica Acta*, *294*, 315–334. https://doi.org/10.1016/j.gca.2020.12.002

Yanez, M. D., LaRowe, D. E., Cable, M. L., & Amend, J. P. (2024). Energy yields for acetylenotrophy on Enceladus and Titan. *Icarus*, *411*, 115969. https://doi.org/10.1016/j.icarus.2024.115969

Zandanel, A., Truche, L., Hellmann, R., Myagkiy, A., Choblet, G., & Tobie, G. (2021). Short lifespans of serpentinization in the rocky core of Enceladus: Implications for hydrogen production. *Icarus*, *364*, 114461. https://doi.org/10.1016/j.icarus.2021.114461